Stratospheric ozone loss in the 1996/1997 Arctic winter: Evaluation based on multiple trajectory analysis for double-sounded air parcels by ILAS

Yukio Terao, Yasuhiro Sasano, Hideaki Nakajima, H. L. Tanaka and Tetsuzo Yasunari

Journal of Geophysical Research, Vol. 107, No. D24, December 27, 2002

Stratospheric ozone loss in the 1996/1997 Arctic winter: Evaluation based on multiple trajectory analysis for double-sounded air parcels by ILAS

Yukio Terao
Institute of Geoscience, University of Tsukuba, Tsukuba, Ibaraki, Japan

Yasuhiro Sasano and Hideaki Nakajima
National Institute for Environmental Studies, Tsukuba, Ibaraki, Japan

H. L. Tanaka and Tetsuzo Yasunari
Institute of Geoscience, University of Tsukuba, Tsukuba, Ibaraki, Japan

Received 9 March 2001; revised 30 August 2001; accepted 3 October 2001; published 1 October 2002.

[1] Quantitative chemical ozone loss rates and amounts in the Arctic polar vortex for the spring of 1997 are analyzed based on ozone profile data obtained by the Improved Limb Atmospheric Spectrometer (ILAS) using an extension of the Match technique. In this study, we calculated additional multiple trajectories and set very strict criteria to overcome the weakness of the satellite sensor data (lower vertical resolution and larger sampling air mass volume) and to identify more accurately a double-sounded air mass. On the average inside the inner edge of the vortex boundary (north of about 70°N equivalent latitude), the local ozone loss rate was 50–80 ppbv/day at the maximum during late February between the levels of 450 and 500 K potential temperatures. The integrated ozone loss during February to March reached 2.0 ± 0.1 ppmv at 475–529 K levels, and the column ozone loss between 400 and 600 K during the 2 months was 96 ± 0.3 DU. Using a relative potential vorticity (rPV) scale, the vortex was divided into some rPV belts, and it was shown that the magnitude of the ozone loss increased gradually toward the vortex center from the edge. The maximum ozone loss rate of 6.0 ± 0.6 ppbv/sunlit hour near the vortex center was higher than near the vortex edge by a factor of 2–3. When we expanded the area of interest to include all the data obtained inside the vortex edge (north of about 65°N equivalent latitude), the local ozone loss rate was about 50 ppbv/day at the maximum. This value is slightly larger than that estimated by the Match analysis using ozonesondes for the same winter by ~10 ppbv/day. Temperature histories of double-sounded air parcels indicated that the extreme ozone loss in the innermost part of the vortex was observed when the air parcel experienced temperatures below T_{NAT} during the two soundings and had experienced temperatures near T_{ice} in the 10 days prior to the first sounding. These facts suggest that the high ozone loss rate deep inside the vortex in the 1997 Arctic early spring correlates with the presence of type Ia polar stratospheric clouds (PSCs). *INDEX TERMS:* 0341 Atmospheric Composition and Structure: Middle atmosphere—constituent transport and chemistry (3334); 0340 Atmospheric Composition and Structure: Middle atmosphere—composition and chemistry; 0394 Atmospheric Composition and Structure: Instruments and techniques; 3360 Meteorology and Atmospheric Dynamics: Remote sensing; 1610 Global Change: Atmosphere (0315, 0325)

Citation: Terao, Y., Y. Sasano, H. Nakajima, H. L. Tanaka, and T. Yasunari, Stratospheric ozone loss in the 1996/1997 Arctic winter: Evaluation based on multiple trajectory analysis for double-sounded air parcels by ILAS, *J. Geophys. Res.*, *107*(D24), 8210, doi:10.1029/2001JD000615, 2002.

1. Introduction

[2] The possibility of ozone depletion due to chlorofluorocarbons (CFCs) was first reported by *Rowland and Molina* [1975], and the Antarctic ozone hole was discovered during the 1980s [*Chubachi*, 1984; *Farman et al.*, 1985]. Since then, phenomenology, processes, and causes of the polar ozone loss have been extensively investigated by many studies on the basis of ground-based, airplane, and satellite remote sensing observations and model simulations [e.g., *WMO*, 1999, and references therein], and the springtime ozone loss has been proved to be a regular phenomenon of the Antarctic stratosphere. A question of primary concern is

0148-0227/02/2001JD000615$09.00

whether, and to what extent, the same or other chemical processes are responsible for destroying ozone in the Arctic polar vortex. Through investigations on the distribution of ozone and ozone-related gases in the Arctic, ozone depletion in the Arctic has been detected throughout the 1990s in the same manner as in Antarctica [e.g., *WMO*, 1999, and references therein].

[3] During the Arctic winter to spring in 1996/1997, total ozone amounts in the northern polar region reached very low levels [*Newman et al.*, 1997]. The meteorological conditions in that winter were different from those of the pervious years, i.e., the late vortex formation and the extremely low temperature in the stratosphere, persisting until late spring [*Coy et al.*, 1997; *Pawson and Naujokat*, 1999]. The chemical ozone depletion inside the polar vortex in the 1997 Arctic spring has been estimated both by observational studies [*Manney et al.*, 1997; *Müller et al.*, 1997; *Knudsen et al.*, 1998; *Sinnhuber et al.*, 1998; *Hansen and Chipperfield*, 1999; *Braathen et al.*, 2000; *Bramstedt et al.*, 2000; *Denis et al.*, 2000; *Schulz et al.*, 2000; *Sasano et al.*, 2000] and by numerical models [*Lefèvre et al.*, 1998; *Guirlet et al.*, 2000].

[4] Quantitative assessment of ozone changes by chemical processes separately from dynamical processes is crucial to improve understanding of the polar stratospheric ozone depletion. In the Arctic region, ozone concentration measured at a fixed location often shows large natural variability due to significant dynamical influences, therefore any estimates of chemical ozone depletion ignoring transports are likely to be affected by the dynamical effects. Although separating the chemical and the dynamical influences on ozone changes is a difficult task and requires careful treatment, a number of methods have been developed for this separation and used to estimate Arctic ozone loss. One such method is known as "Match" [*von der Gathen et al.*, 1995; *Rex et al.*, 1997, 1998, 1999; *Schulz et al.*, 2000], which uses pairs of ozonesonde profiles ("matches") obtained at separated locations but identified by Lagrangian trajectory analysis to have traced the same air mass. By this approach, the dynamical effect in ozone changes can be neglected and only chemical changes remain between the first and the second observations of each matching pair, so that the chemical ozone loss rate and amount can be estimated quantitatively in several Arctic winters.

[5] We applied a similar technique to the ozone profile data obtained with the satellite-borne sensor, Improved Limb Atmospheric Spectrometer (ILAS) on board the Advanced Earth Observing Satellite (ADEOS) [*Sasano et al.*, 1999; *Nakajima et al.*, 2002], and presented preliminary estimates of the ozone loss rates and amounts during the Arctic spring of 1997 [*Sasano et al.*, 2000] and the nitric acid change rates at the same time [*Terao et al.*, 2000]. There are two advantages in using the ILAS data over the Match analysis: (1) ILAS provides data not only regarding ozone but also nitric acid, passive tracers, aerosol extinction coefficient and so on and (2) ILAS can make measurements with the same quality homogeneously over an entire narrow zone at high latitude (Figure 1). On the other hand, there is a problem regarding conservation of air masses due to a relatively low vertical resolution and a larger sampling air mass volume of the satellite sensor than the ozonesonde data. In order to overcome this weakness of the satellite sensor data, we introduce much stricter criteria than those of the sonde-Match, to identify more reliably double-sounded air parcels.

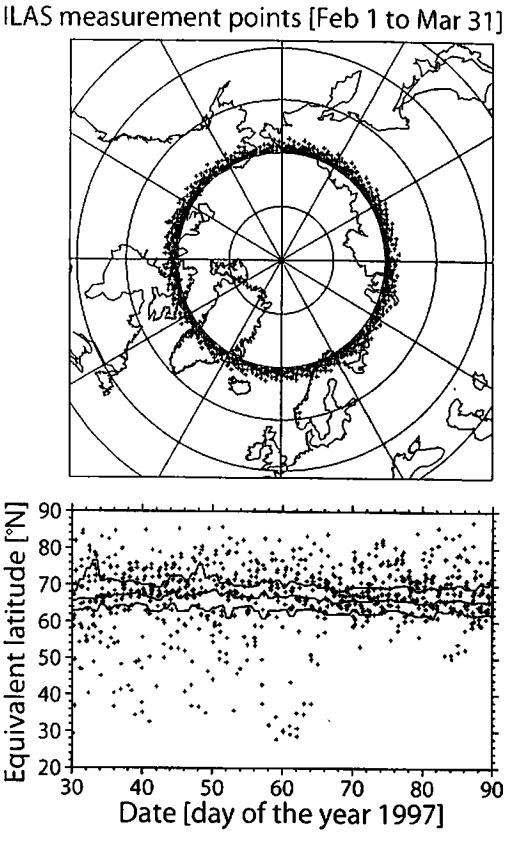

Figure 1. Location of ILAS measurement points on a geographic map (top panel) and a time-equivalent latitude section of the measurements on a 475 K potential temperature surface (bottom panel) in Northern Hemisphere from 1 February to 31 March 1997. Thick and thin solid curves in the bottom panel indicate the vortex edge and the vortex boundary region, respectively.

[6] In this study we propose the Satellite-Match analysis method and reanalyze quantitative chemical ozone loss rates and amounts in the Arctic polar vortex for the spring of 1997. To determine the chemically induced ozone loss accurately, we use the newest products of ILAS (version 5.20) and the improved analysis method for double-sounded air parcels based on multiple trajectories. This study presents vortex-averaged ozone loss rates and distribution of ozone loss inside the vortex, and discusses the relationship between the ozone loss and temperature history of the air masses.

[7] This paper consists of six sections. In section 2 we describe the ILAS data and meteorological data used in this study. Section 3 presents the method of the Satellite-Match analysis, and describes in detail the calculation of multiple trajectories, criteria for selecting double-sounded air parcels, and algorithm for calculating chemical ozone loss rates. Section 4 shows vortex-averaged ozone loss rates and changes of ozone loss rate with respect to relative position in the vortex, as well as temperature history along the trajectory of a corresponding double-sounded air parcel. We discuss the results in section 5, which includes a sensitivity test of ozone change rate to the diabatic descent and to the criteria for selecting double-sounded air parcels, the relation-

ship between the ozone loss and low temperature experienced by the air mass, and a comparison of the ozone loss rates with other studies. This study is summarized in section 6.

2. Data

[8] ILAS is a solar occultation sensor and provides vertical profiles of gas species (ozone, nitric acid, nitrogen dioxide, methane, nitrous oxide, and water vapor) by infrared spectrometry and aerosol extinction coefficient by visible spectrometry [*Sasano et al.*, 1999; *Nakajima et al.*, 2002]. The present analysis uses the ozone mixing ratio profiles obtained by the version 5.20 ILAS retrieval algorithm [*Yokota et al.*, 2002]. Figure 1 (top panel) depicts the locations of the ILAS measurements on a geographic map in the Northern Hemisphere from 1 February to 31 March 1997, during which period 735 ozone profiles were obtained. The ILAS measurements were made only between 63°N and 70°N but covered all longitudinal regions. Figure 1 (bottom panel) shows the distributions of the ILAS measurements, the vortex edge, and the vortex boundary region as functions of date and equivalent latitudes [*Nash et al.*, 1996] at a 475 K potential temperature surface. The vortex edge and the vortex boundary region were defined on each day by a similar method to that of *Nash et al.* [1996]. Throughout the 2 months ILAS made large numbers of observations inside the poleward (inner) edge of, within the boundary region of, and outside the equatorward (outer) edge of the polar vortex.

[9] Although the quality of the version 5.20 ILAS data is described by *Yokota et al.* [2002], we briefly summarize them here. The estimated root-sum-square total uncertainties in ozone values are 14%, 9%, and 5% at 15 km, 20 km, and 25 km, respectively, on the average in the Northern Hemisphere from November 1996 to June 1997. These errors are associated mainly with residuals of the nonlinear least squares fitting of the simulated transmittance to the observed transmittance in the retrieval. Measurement repeatability, defined as a relative standard deviation of ozone values obtained during 3–5 days in quiescent periods (e.g., around the South Pole in summer), is 7% at 15 km and 3% at 20 km. These values are smaller than the root-sum-square total uncertainties and should represent measurement precisions. Note that the ILAS gas values could have been biased even after applying the "nongaseous correction" [*Yokota et al.*, 2002] when polar stratospheric clouds (PSCs) existed at the same time. Numerical simulations show that the ozone values may have a very large positive bias of 0.90 ppmv (or a small negative bias of 0.16 ppmv) at 20 km if ice (or nitric acid trihydrate (NAT)) PSCs having such a large extinction coefficient as 1×10^{-3} km^{-1} exist. Thus, care should be taken especially when ILAS observed ice PSCs. In this study we eliminated all the ozone data that may have been affected by PSCs occurrence, according to the information on PSCs detection provided by *Saitoh et al.* [2002].

[10] The version 5.20 ILAS ozone data have been validated against the ozone data obtained by ozonesondes, instruments on board balloons and aircrafts, and ground-based instruments, as well as by the satellite sensors, Halogen Occultation Experiment (HALOE), Stratospheric Aerosol and Gas Experiment (SAGE) II, and Polar Ozone and Aerosol Measurement (POAM) II [*Sugita et al.*, 2002]. The ILAS ozone data generally agree with them within ±10%. Focusing on the winter in the Northern Hemisphere, the relative differences in comparison with the ozonesonde data are 14% at 11–15 km and 8% at 16–20 km during February, and 7% at 11–15 km and 5% at 16–20 km during March.

[11] The following procedure is used in handling the ILAS ozone mixing ratio profiles. Though the time of ILAS measurements is precisely determined in the order of 10 ms, we treat it in units of hour by rounding up to every hour for convenience, because the time step of trajectory analysis is 1 hour (described later). Representative time and geometrical location of the observations are provided for the tangent height of 20 km. Note that changes in time and location of the measurement within each sounding are small enough to be neglected. As the ILAS ozone data are provided as a function of geometrical altitude with 1 km intervals, the vertical coordinate is transformed to a potential temperature coordinate by using the United Kingdom Meteorological Office (UKMO) assimilation data [*Swinbank and O'Neill*, 1994] and the ILAS ozone mixing ratios are interpolated on potential temperature surfaces.

[12] The UKMO assimilation data are also used for meteorological analysis and trajectory calculations. The data are provided daily on a grid of 2.5 degrees in latitude and 3.75 degrees in longitude on 22 Upper Atmosphere Research Satellite (UARS) standard pressure levels at 1200 UT.

3. Analysis Method

[13] A double-sounded air parcel that the ILAS sounded twice at different locations and at different times (match pair) is searched from the ILAS data set with 10-day forward isentropic trajectories, and a change of ozone mixing ratio is calculated from the two profiles of the air parcel taking the diabatic descent effects [*Knudsen et al.*, 1998] into consideration. The analysis is done at nine isentropic levels from 375 to 550 K at 25 K intervals, and 600 K.

3.1. Trajectory Analysis

[14] Trajectory analysis is conducted with an isentropic Lagrangian model which was supplied by UKMO (R. Swinbank, private communication). The main specifications of the trajectory model are as follows: The integration in calculating trajectory is done by the fourth-order Runge-Kutta scheme with 1-hour interval. The time interpolation and the space interpolation with respect to the horizontal direction are done linearly, and the vertical interpolation is done linearly with respect to the log-P coordinate.

[15] Our previous analysis [*Sasano et al.*, 2000] was based only on a single forward trajectory, which started from each ILAS observation point (location 1) for searching a matching observation (location 2). In the sonde-Match analysis, a single forward trajectory was used for searching a match in the 1991/1992 winter [*von der Gathen et al.*, 1995; *Rex et al.*, 1998] and six additional forward trajectories around each sonde measurement point were introduced to check the accuracy of matches in the 1994/1995 winter [*Rex et al.*, 1999]. Since satellite sensor data have a relatively low vertical resolution (ILAS has a vertical resolution of about 2 km) and larger sampling air mass volume than the ozonesonde data, a strict criterion for assuring conservation of air masses needs to be introduced to identify a double-sounded air mass more reliably.

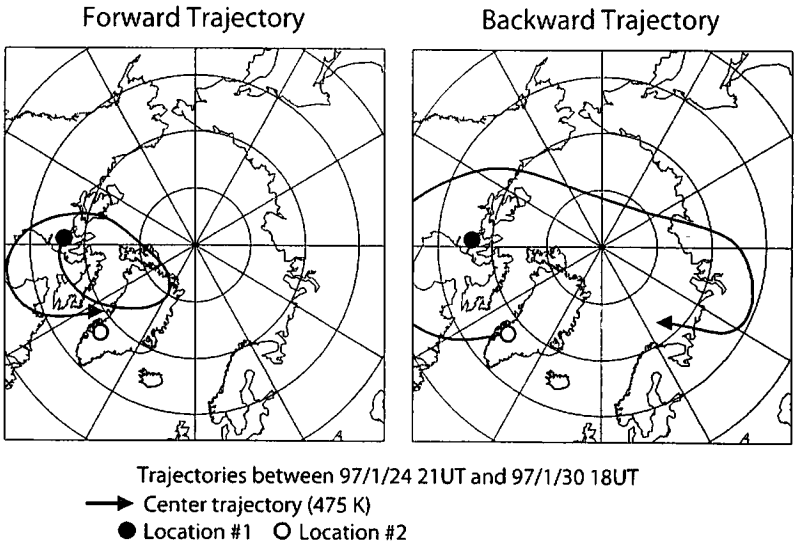

Figure 2. Example of a single forward (left) and a single backward (right) trajectory on the 475 K potential temperature surface between 24 and 30 January 1997. The first ILAS measurement point (location 1) is marked by a solid circle and the second point (location 2) by an open circle.

[16] For this purpose, we also calculate a backward trajectory which starts from location 2. Figure 2 shows an example of a pair of forward and backward trajectories on the 475 K potential temperature surface. As shown in Figure 2, the forward trajectory which starts from location 1 matches well with location 2, however, the backward trajectory from location 2 never gets close to location 1. This type of case should be avoided when identifying double-sounded air parcels.

[17] Furthermore, we consider a cluster of forward trajectories which start from around location 1 and a cluster of backward trajectories from around location 2. The initial volume of the cluster is intended to represent a finite sampling air mass volume of ILAS. Figure 3 presents a schematic picture of ILAS sampling air mass volume (1.6 km in height and 300 km in distance as representative values) and the corresponding multiple trajectories. We calculate four additional trajectories which start from points separated by ±150 km along the line of sight on the two surfaces separated by ±0.8 km in altitude around each ILAS observation point at its tangent height. In total, ten trajectories (a central single forward/backward trajectory and a cluster of four forward/backward trajectories) are calculated for each ILAS measurement at each level, as shown in Table 1.

[18] Figure 4 illustrates an example of the cluster of forward/backward trajectories. The thick black curve shows the central trajectory on the 475 K potential temperature surface, and blue and red trajectories are at the upper level (493 K) and at the lower level (457 K), respectively. Locations 1 and 2 can be identified as a double-sounded air parcel both by the forward and backward central trajectories in this case. However, there are large differences between the upper and lower level trajectories, and the locations of the end point of each trajectory are quite different, which can be explained by a large vertical shear

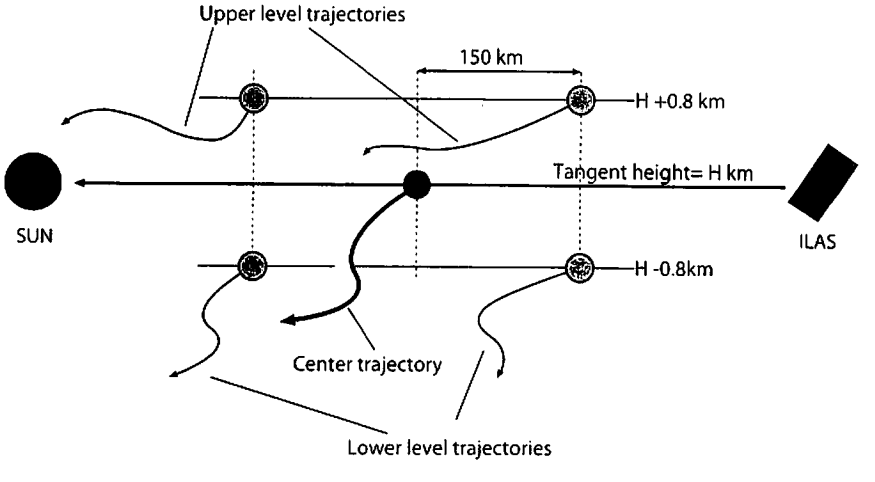

Figure 3. Schematic picture of ILAS sampling air mass volume and a corresponding cluster of trajectories.

Table 1. Trajectory Calculation Levels

Potential temperature, K	Approximate altitude,[a] km	+0.8 km level,[a] K	−0.8 km level,[a] K
375	13.6	387.8	361.9
400	15.0	413.6	386.6
425	16.4	440.1	410.4
450	17.7	466.7	433.9
475	18.9	493.1	457.4
500	19.9	519.3	481.2
525	20.9	545.5	505.1
550	22.2	571.8	529.0
600	23.6	624.6	576.4

[a] Three months mean during February, March, and April.

in the wind field. Also, as shown in the right-hand panel of Figure 4, there are large differences between the two trajectories on the same surface, which are caused by a large horizontal shear in the wind field. As such, if four multiple forward/backward trajectories diverge significantly, this pair of measurements should not be regarded as a double-sounded air parcel. Figure 5 indicates an example showing that all of the multiple forward and backward trajectories are very compact during 7 days, so we can reliably assume this is a double-sounded air parcel.

3.2. Identification Criteria of Double-Sounded Air Parcel

[19] We set several criteria for identifying reliable double-sounded air parcels.

1. The distance (referred to as a forward match radius) between the position of location 2 and the central forward trajectory which starts from location 1, which corresponds to the distance between the large open circle and the tip of the thick solid arrow in the left-hand panel of Figure 5, should be less than 500 km.

2. The distance (referred to as a forward cluster radius) between the position of location 2 and all four forward trajectories which start from around location 1, which corresponds to the distance between the large open circle and each small solid or open circle in the left-hand panel of Figure 5, should be less than 1600 km.

3. The same criteria are applied to the backward trajectory analysis. Thus a backward match radius should be less than 500 km and a backward cluster radius less than 1600 km.

4. The difference between the maximum and the minimum value of potential vorticity (PV) along the central forward trajectory, to which a 24-hour running mean was applied (referred as ΔPV), should be less than 20%.

[20] These criteria were chosen on the basis of error analysis similar to that by *Rex et al.* [1998, 1999]. Figure 6 shows a standard deviation of ozone mixing ratio change as a function of forward match radius and backward match radius, in which the ozone change is corrected by an expected ozone change along the trajectory. The expected ozone change was calculated by multiplying the sunlit time along the trajectory by the ozone change rate per sunlit time (the way of determining the ozone change rate by regression analysis is described in the next section.). Thus Figure 6 indicates the dependence of a residual ozone change from the regression line, namely, an error, on the distance criterion. If a larger distance criterion is used, the error becomes larger, and conversely, if a smaller distance is used, the number of double-sounded air parcels is too small to calculate ozone change rates in a statistically meaningful way. Therefore, 500 km was chosen as the criterion for the present analysis. The criteria of the forward/backward cluster radius and ΔPV were determined in the same manner as the forward/backward match radius.

[21] Table 2 shows the total number of double-sounded air parcels inside the inner edge of the vortex boundary selected according to the criteria during February and March

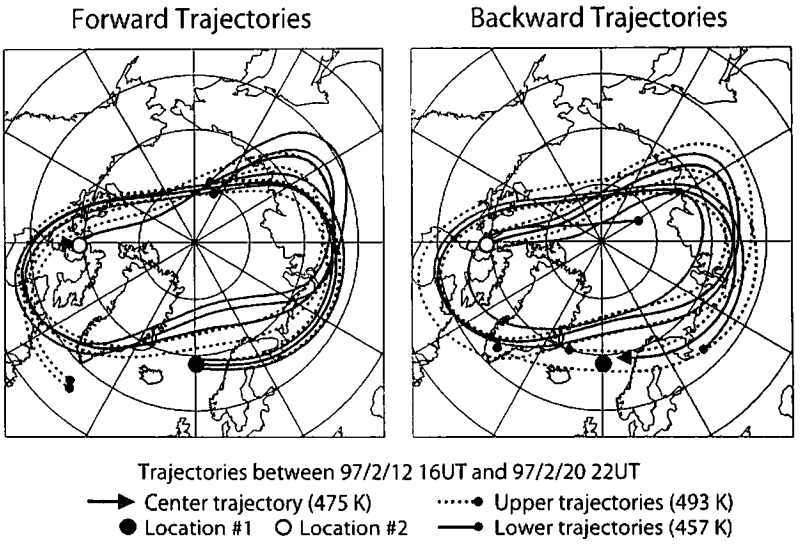

Figure 4. Example of a cluster of forward (left) and backward (right) trajectories between 12 and 20 February 1997. A thick black curve with an arrow shows a center trajectory on the 475 K potential temperature surface. Blue and red trajectories are at the upper level (493 K) and the lower level (457 K), respectively, and small solid circles show the end of each trajectory. See color version of this figure at back of this issue.

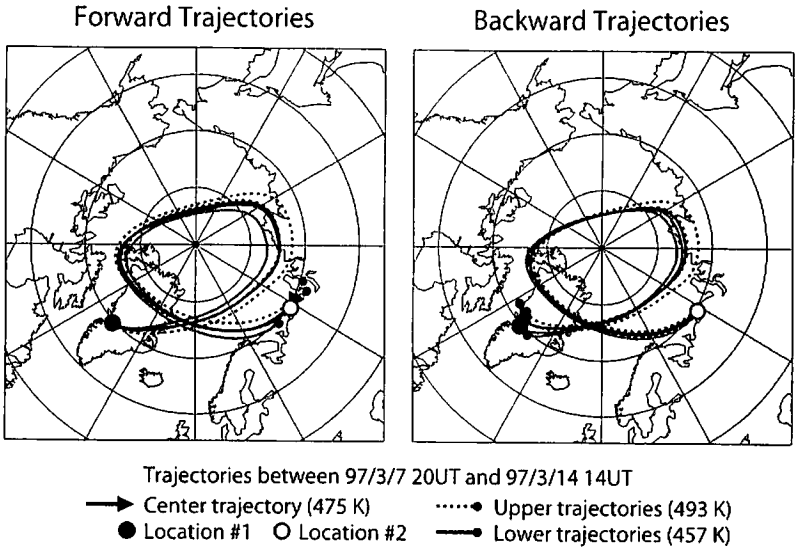

Figure 5. Same as in Figure 4, but between 7 and 14 March 1997. See color version of this figure at back of this issue.

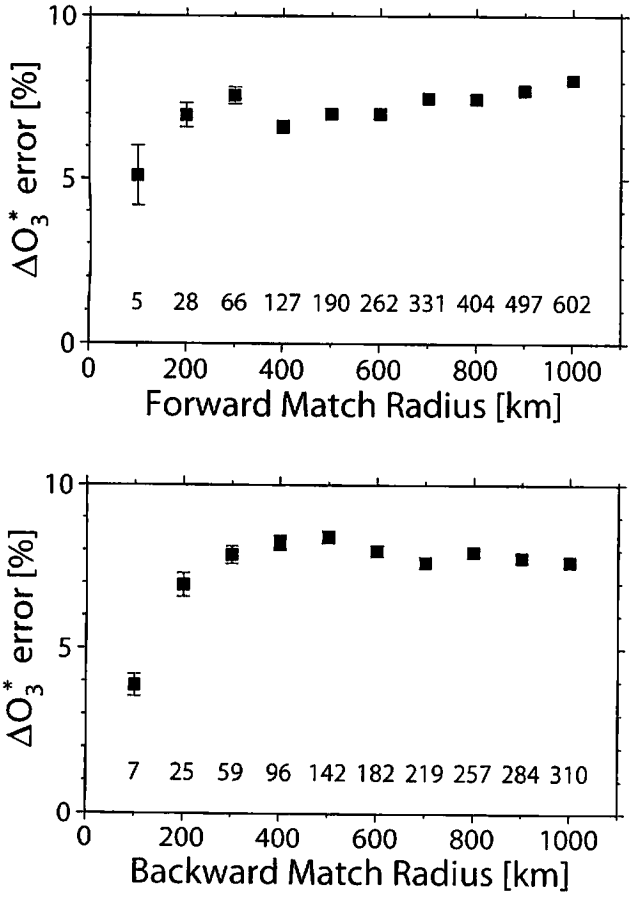

Figure 6. Standard deviation of ozone mixing ratio change, which is corrected by the expected ozone loss along the trajectory, as a function of the forward match radius (top panel) and backward match radius (bottom panel). The data used here were obtained during 4 February to 5 March on the 475 K potential temperature surface. The figures at the bottom indicate the number of double-sounded air parcels selected for each match radius criterion.

between 400 and 600 K potential temperature surfaces. If we considered only forward match radius and ΔPV, more than one thousand double-sounded air parcels were obtained (row 1 in Table 2). When we added the backward match radius criterion, the number of double-sounded air parcels was approximately half. By considering all of the criteria described above, several hundred double-sounded air parcels were identified for each month (row 3 in Table 2), which, although they are less than one third of the number determined only by the forward match radius, are enough to statistically calculate ozone change rates. We cannot obtain enough double-sounded air parcels at the 375 K levels inside the vortex, thus the following analysis was done for the vertical range from 400 to 600 K surfaces.

3.3. Calculation of Ozone Change Rate

[22] A change in ozone mixing ratio (referred as ΔO_3) is calculated, by considering changes in potential temperature by diabatic effects (referred as $\Delta\theta$), as $\Delta O_3 = O_3(\theta + \Delta\theta)_{\text{location 2}} - O_3(\theta)_{\text{location 1}}$, where $O_3(\theta)$ means an ozone mixing ratio at a θ potential temperature level and the subscript indicates a location of ILAS observation. Thus, the ozone mixing ratio at location 2 is modified by potential temperature changes due to diabatic cooling during the flight time. The diabatic cooling rates averaged over the polar vortex were taken from the work of *Knudsen et al.* [1998].

[23] A statistical treatment is applied to the subset of double-sounded air parcels to calculate ozone change rates for each day. Each subset consists of double-sounded air parcels that are gathered within 7 days before and after each

Table 2. Total Number of Double-Sounded Air Parcels Between 400 and 600 K Potential Temperature Surfaces for Corresponding Criteria During February and March

Criteria	February	March
1 Forward match radius ≤ 500 km and ΔPV ≤ 20%	1426	2179
2 1 + backward match radius ≤ 500 km	735	891
3 2 + forward and backward cluster radius ≤ 1600 km	565	654

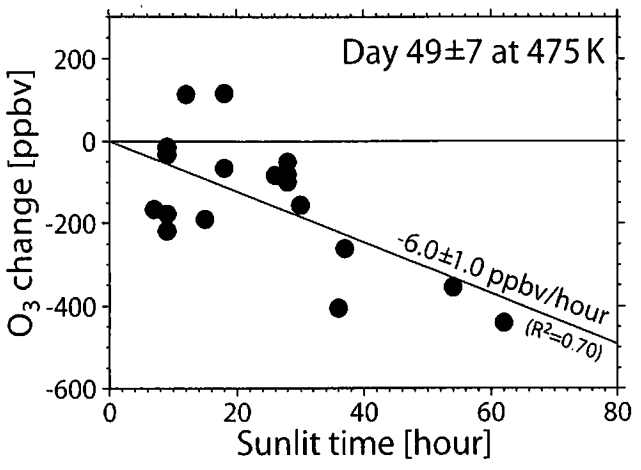

Figure 7. Scatterplot for ozone mixing ratio change as a function of sunlit time along the trajectory. The data used here were obtained during 11–25 February on the 475 K potential temperature surface. A regression coefficient estimated as −6.0 ± 1.0 ppbv/sunlit hour is referred to as an ozone change rate on 18 February. The coefficient of determination (R^2) is 0.70.

target day. Assuming that ozone changes are linearly proportional to the sunlit time along the trajectory, a proportional coefficient (ozone change against sunlit time) is calculated using the least squares method from each subset of data. Figure 7 is a scatterplot for ozone mixing ratio changes of double-sounded air parcels as a function of sunlit time along their trajectories. The regression line gives an ozone change rate in ppbv per sunlit hour. The data used in this figure were obtained inside the inner edge of the vortex boundary region during 11–25 February on the 475 K potential temperature surface, and the regression coefficient, −6.0 ± 1.0 ppbv/sunlit hour, is referred to as the ozone change rate against sunlit time on 18 February.

[24] The present technique assumes that contributions by dynamical effects can be eliminated and only changes in ozone due to photochemical reactions are derived [*von der Gathen et al.*, 1995]. To check this, we conducted a bivariate regression analysis allowing ozone changes during nighttime [*Rex et al.*, 1998, 1999; *Sasano et al.*, 2000]. The results show that the ozone change rates from 4 February to 6 March on the 475 K potential temperature surface are −5.1 ± 1.9 ppbv/sunlit hour and 0.3 ± 1.0 ppbv/dark hour. This shows that the ozone change during nighttime is almost zero, and implies that the ozone change due to dynamical effects can be neglected.

4. Results

4.1. Ozone Change Rate Averaged Inside the Inner Vortex Edge

[25] Figure 8 shows the location of double-sounded air parcels as functions of date and PV (top panel), and equivalent latitude (bottom panel) on the 475 K potential temperature surface. The PV change in each individual double-sounded air parcel is shown to be conserved within 20% level because of the constraint by the match criterion of $\Delta PV \leq 20\%$. The equivalent latitude of each air parcel looks to change more significantly than the PV. This is simply because the maximum PV value at the center of the vortex is variable with time. Figure 8 also shows the vortex edge (thick line), and inner (poleward) and outer (equatorward) edges of the vortex boundary region (thin lines). In this subsection we use the double-sounded air parcels (two crosses linked by a line in the figure) only inside the inner edge of the vortex boundary, which was located at around 70°N equivalent latitude (corresponding approximately to 45 PVU, 1 PVU = 10^{-6} km^2 s^{-1} kg^{-1}) on the average. We define the ozone change rate derived from this data set as a "vortex-averaged" value inside the inner vortex edge.

[26] The ozone change rate in ppbv per sunlit hour can be converted to a quantity of ozone change per day by multiplying them with an averaged sunlit time (hours) for each day. The sunlit time for each day can be calculated as the average of sunlit time experienced by the air parcels on trajectories of interest. In addition, the net ozone change for 2 months can be evaluated by integrating the ozone change per day with time. In this calculation, the altitude change due to diabatic descending motion of the air parcels is taken into consideration.

[27] Figure 9a shows the ozone change rates (ppbv/day) averaged inside the inner edge of the vortex boundary as a function of potential temperature and date, which is

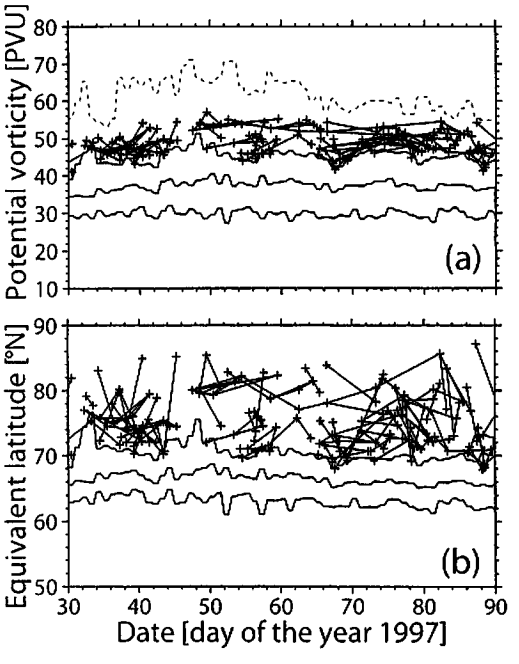

Figure 8. Location of double-sounded air parcels obtained inside the inner edge of the vortex boundary as a function of date (day of the year 1997) and PV (top panel) and equivalent latitudes (bottom panel) on the 475 K potential temperature surface. ILAS observation points are marked by crosses, and two matching observations are connected by a solid line. Thick and thin solid curves in both panels show the vortex edge and the poleward (inner) and equatorward (outer) edges of the vortex boundary region, respectively. A dashed curve in the top panel shows the maximum PV in the vortex, which defines the center of the vortex.

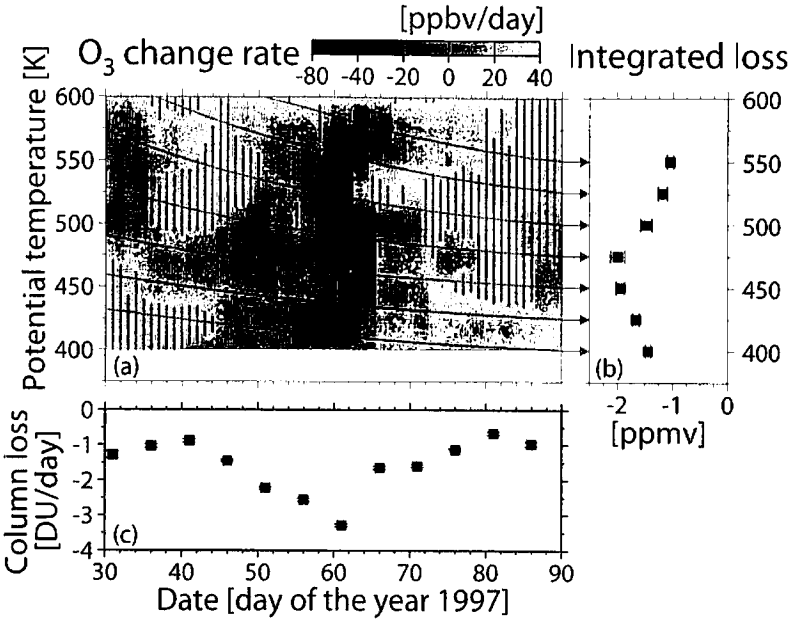

Figure 9. (a) Color-coded ozone change rates (in ppbv per day) inside the inner edge of the vortex boundary (north of about 70 °N equivalent latitude) as a function of potential temperature and date. Vertical bars indicate the region with statistical significance less than 99%. Smooth thin curves show potential temperature changes of air parcels (diabatic descent of air masses) (adopted from the work of *Knudsen et al.* [1998]). (b) Integrated ozone changes from 30 January (day 30) to 31 March (day 90) along the descending motion due to diabatic cooling. For the integration, ozone change rates are vertically interpolated by a cubic spline. For the uppermost two levels, days 51–90 and days 37–90 are used for the integration, respectively. Error bars represent 1 sigma. (c) Ozone column change rates (in DU per day), which are obtained by integrating local ozone change rates (in number density per day) from 400 to 600 K. Results are plotted every 5 days. See color version of this figure at back of this issue.

derived from the set of double-sounded air parcels shown in Figure 8. Ozone losses take place at almost all altitudes during February and March, with particularly large losses during late February, where the local maximum ozone loss rate is 50–80 ppbv/day at 450–500 K potential temperature levels. The local ozone loss rates as derived here are 10–20 ppbv/day higher than those obtained by our preliminary analysis [*Sasano et al.*, 2000]. The difference in the ILAS product version (*Sasano et al.* [2000] used Version 3.10 whereas the present study used Version 5.20) is relatively small for the ozone products. A probable cause for the higher ozone loss rates is the stricter criteria used for identifying the double-sounded air parcels (discussed further in section 5.1). Vertical bars in the figure indicate the region with statistical significance lower than 99% by the t-value test. Although some regions with ozone gain (yellow color) appeared in early February and late March, they have no statistical significance.

[28] Figure 9b shows the integrated ozone change from 30 January (day 30) to 31 March (day 90) along the potential temperature changes of air parcels which were illustrated by the smooth thin curves in panel (a). Note that the integration for the uppermost two levels was done for days 51–90 and days 37–90, respectively. The integrated ozone loss reaches the maximum of 2.0 ± 0.1 ppmv on the surface that reached the 475 K level on 31 March from the 529 K on 30 January. This is about 55% of the initial vortex-averaged ozone concentration (3.6 ppmv on 30 January at the 529 K level).

[29] Furthermore, the column ozone change per day is shown in Figure 9c, where the ozone change rate in number density per day at each level was integrated from 400 to 600 K. Monthly mean temperature and pressure profiles inside the inner vortex edge were used to convert from mixing ratio to number density in the unit of ozone change rate. The column ozone loss during the 2 months is 96 ± 0.3 DU.

4.2. Ozone Change Rate as a Function of rPV

[30] In order to investigate the relationship between ozone loss and location relative to the vortex, we used a relative PV (rPV) scale [*Rex et al.*, 1998, 1999; *Schulz et al.*, 2000]. The rPV ranges from 0 corresponding to the center of the vortex, where the PV value takes the maximum, to 1 corresponding to the vortex edge. The rPV is scaled so that equal intervals in rPV correspond to equal area fractions of the vortex each day. The vortex is divided into rPV belts with their centers at 0.1, 0.2, 0.4, 0.6, 0.8, and 1.0, and with a width of 0.4. An exception is a width of 0.2 for the rPV belt centered at 0.1. Double-sounded air parcels which fall in each belt are defined so that the rPVs at locations 1 and 2 are both situated in that belt. Figure 10 shows the location of double-sounded air parcels as a function of rPV. The colors discriminate the rPV belts. For example, the 0.4 rPV belt contains the double-sounded air parcels whose rPVs both at location 1 and at location 2 are between 0.2 and 0.6. The number of double-sounded air parcels inside the inner edge of the vortex boundary (corresponding to about 0.6 rPV on the average) became smaller than that for the vortex-averaged analysis

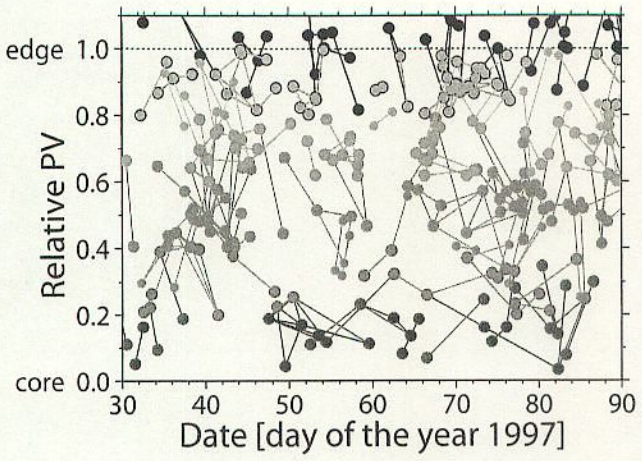

Figure 10. Location of double-sounded air parcels obtained in each rPV belt. In the rPV scale, 0 refers to the center of the vortex where the PV value takes the maximum and 1 refers to the vortex edge (see text). Red, magenta, orange, green, cyan, and blue indicate the double-sounded air parcels in the rPV belts of 0.0–0.2, 0.0–0.4, 0.2–0.6, 0.4–0.8, 0.6–1.0, and 0.8–1.2, respectively. See color version of this figure at back of this issue.

(section 4.1) because we selected only double-sounded air parcels found just within each 0.4 rPV belt.

[31] Figure 11 shows ozone change rates (ppbv/sunlit hour) as a function of rPV. The ozone change rate is calculated by regression analysis using a subset of double-sounded air parcels for each rPV belt from 4 February to 6 March at the 475 K level, where a large negative ozone change rate (loss) was observed (Figure 9). The ozone loss increases with a decrease in rPV from the vortex edge toward the vortex center, showing a step-like increase at 0.6 and 0.2 rPVs (approximately 73°N and 80°N equivalent latitude, respectively). The maximum ozone loss is 6.0 ± 0.6 ppbv/sunlit hour at 0.2 rPV near the vortex center. Even at the vortex edge ozone loss occurred (2.7 ± 1.2 ppbv/sunlit hour). The results indicate that the magnitude of ozone loss depends on rPV within the vortex and that the ozone loss near the vortex center is larger than near the vortex edge by a factor of 2–3.

[32] By integrating ozone change rates from the vortex center (0.0 rPV) to the inner vortex edge (0.66 rPVs), the ozone change rate averaged inside the inner vortex edge can be estimated as −5.0 ± 0.9 ppbv/sunlit hour, which can be regarded as an average value from 4 February to 6 March at the 475 K level. For the integration, ozone change rates are interpolated with the rPV by a cubic spline. To compare this with the ozone change rate previously derived in section 4.1, we recalculated the "vortex-averaged" ozone change rate with the same period at the same level using the data on Figure 9. The ozone change rate inside the inner vortex edge thus calculated is −45.0 ± 8.7 ppbv/day, which can be converted to −5.1 ± 1.0 ppbv/sunlit hour. This is comparable to the value derived above although the ways of average calculations are different.

4.3. Ozone Change Rate Averaged Within the Whole Vortex

[33] As shown in section 4.2, the magnitude of ozone loss are strongly dependent on relative location to the vortex in the winter 1996/1997. Thus the "vortex-averaged" ozone loss rate may be influenced by the area of the vortex where the average ozone loss rate is calculated. Figure 12 shows, for comparison, two time series of ozone change rates (ppbv/day) at 475 K that are calculated with the method described in section 4.1 using the data obtained inside the inner edge of the vortex boundary (squares), and inside the vortex edge (diamonds). The former represents the ozone change rates as averaged over north of about 70 °N equivalent latitude, and the later represents those over north of about 65 °N equivalent latitude (approximately 37 PVU). Figure 12 shows the ozone loss rates derived from the data inside the vortex edge are 40–50 ppbv/day during late February, and lower than 50–60 ppbv/day derived from the subset of the data inside the inner vortex edge. This is because the calculation of the ozone loss rates inside the vortex edge include the data for the region between 65 °N and 70 °N equivalent latitudes where the ozone loss is relatively small. Inside the vortex edge, the integrated ozone change during the 2 months is 1.6 ± 0.1 ppmv on the 475–529 K surfaces and the column ozone loss between 400 and 600 K surfaces during the 2 months is 72 ± 0.4 DU. These results are also smaller than the analysis for inside the inner vortex edge.

4.4. Temperature History Along the Trajectory

[34] In this section, we show two temperature histories along the trajectories of a double-sounded air parcel: One is along a central forward trajectory between location 1 and

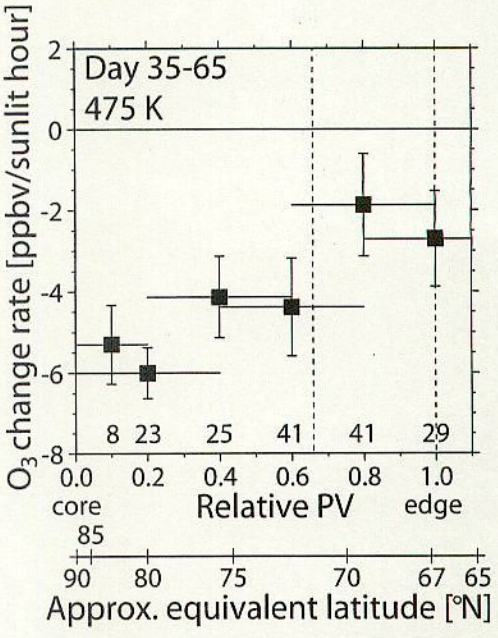

Figure 11. Ozone change rates (in ppbv per sunlit time) as a function of rPV. Each data point is calculated by regression analysis for double-sounded air parcels obtained in the rPV belts of 0.0–0.2, 0.0–0.4, 0.2–0.6, 0.4–0.8, 0.6–1.0, and 0.8–1.2, respectively, from 4 February to 6 March at 475 K. Figures at the bottom indicate the number of double-sounded air parcels used for the calculation. Vertical error bars represent 1 sigma. A scale for approximate equivalent latitude is also plotted. Vertical dashed lines show the vortex edge (1.0 rPV) and the inner edge of the vortex boundary (0.66 rPV) on the average.

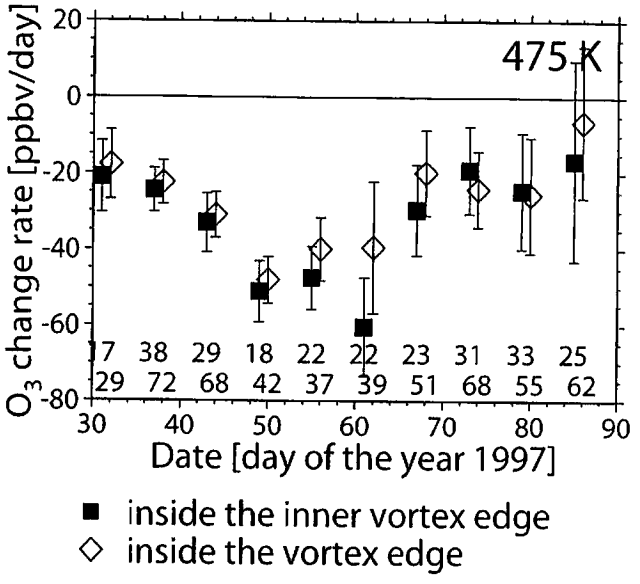

Figure 12. Time series of ozone change rates (in ppbv per day) on the 475 K potential temperature surface. Solid squares give the ozone change rates as calculated using the data obtained inside the inner edge of the vortex boundary (north of about 70 °N equivalent latitude), and open diamonds give the ozone change rates using the data inside the vortex edge (north of about 65 °N equivalent latitude). Figures near the bottom show the number of double-sounded air parcels inside the inner edge of the vortex boundary (row 1) and inside the vortex edge (row 2). Results are plotted every 6 days. Diamonds are shifted horizontally for the sake of clarity. Error bars denote 1 sigma.

location 2 (called TH-F) and the other is along a 10-day central backward trajectory which started from location 1 (TH-B). When the ozone loss is observed in the double-sounded air parcel, TH-F indicates the temperature history of the air parcel while the ozone loss is occurring, and TH-B indicates that before the ozone loss occurs.

[35] Figure 13 shows the minimum temperatures found in TH-F (a) and TH-B (b) for the air parcels inside the inner edge of the vortex boundary (corresponding to the trajectories used to calculate the ozone change rates in Figure 9). The minimum temperatures were searched for both on TH-F and TH-B for each double-sounded air parcel, and were averaged within 7 days before and after each target day in a similar way to that used for calculating the ozone change rate. The distribution patterns of the minimum temperatures from TH-F and TH-B are very similar to each other, but the minimum temperature on TH-B is by about 5 K lower than on TH-F. This difference may result from the geographical differences in the route of the trajectories (described later). Focusing on the regions between 450 and 550 K potential temperatures during late February, where the large ozone loss was observed, the temperature drops below 195 K on TH-F and below 190 K on TH-B.

[36] Figure 14 plots the minimum temperatures (solid square) and the maximum temperatures (open diamond) from TH-F (a) and TH-B (b) as a function of the rPV. The frost temperature of ice (T_{ice}) [*Marti and Mauersberger*, 1993], the equilibrium temperature of NAT (T_{NAT}) [*Hanson and Mauersberger*, 1988], and the melting temperature of sulfuric acid tetrahydrate (T_{SAT}) [*Middlebrook et al.*, 1993] were calculated using the monthly mean and standard deviation of water vapor and nitric acid mixing ratios at 475 K measured by ILAS inside the vortex during February (5.5 ± 0.3 ppmv H_2O and 10.5 ± 0.2 ppbv HNO_3). T_{ice}, T_{NAT}, and T_{SAT} vary within ±0.5 K corresponding to the standard deviations in the water vapor and nitric acid mixing ratios. Furthermore, the UKMO temperatures at the NAT point were reported to be higher than the radiosonde temperatures by 1.7 K at 475 K with a standard deviation of about 2 K, from comparisons of the UKMO lower stratospheric temperatures with those obtained by the radiosondes during the winter of 1994/95 [*Pullen and Jones*, 1997]. If the same positive bias exists in the 1996/1997 winter, it also may be a cause of uncertainty in the following analysis.

[37] The ozone loss increases from the vortex edge to the vortex center (Figure 11) while the minimum temperatures on the temperature history (TH-F and TH-B) decreases (Figure 14). Furthermore, a stepwise structure at 0.2 rPV is seen both in the ozone change rate and in the temperature history. In the vortex core region (0.1 and 0.2 rPV belts), where the ozone loss is large, the minimum temperature on TH-B drops near T_{ice} and that on TH-F drops well below T_{NAT}. This means that the large ozone loss is observed in the deep part of the vortex when the double-sounded air parcels

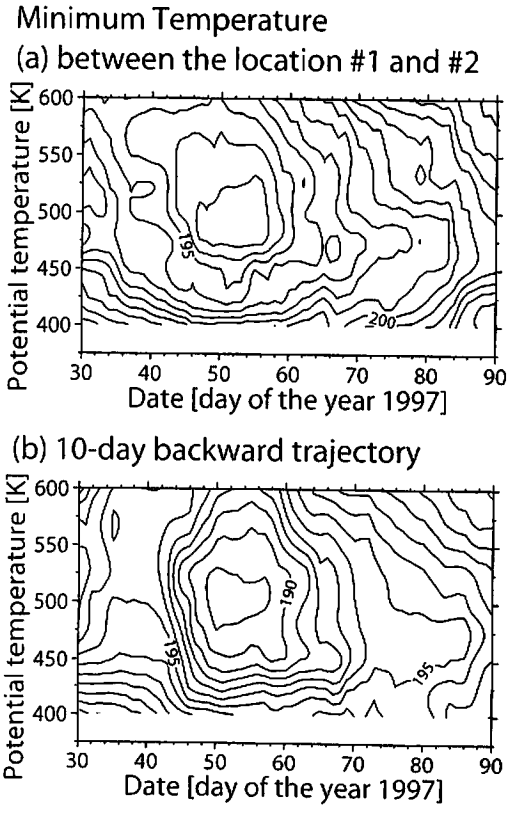

Figure 13. Minimum temperatures along (a) a central forward trajectory between locations 1 and 2 and (b) a 10-day central backward trajectory, which started from location 1 for double-sounded air parcels inside the inner edge of the vortex boundary as a function of potential temperature and date. The contour interval is 1 K.

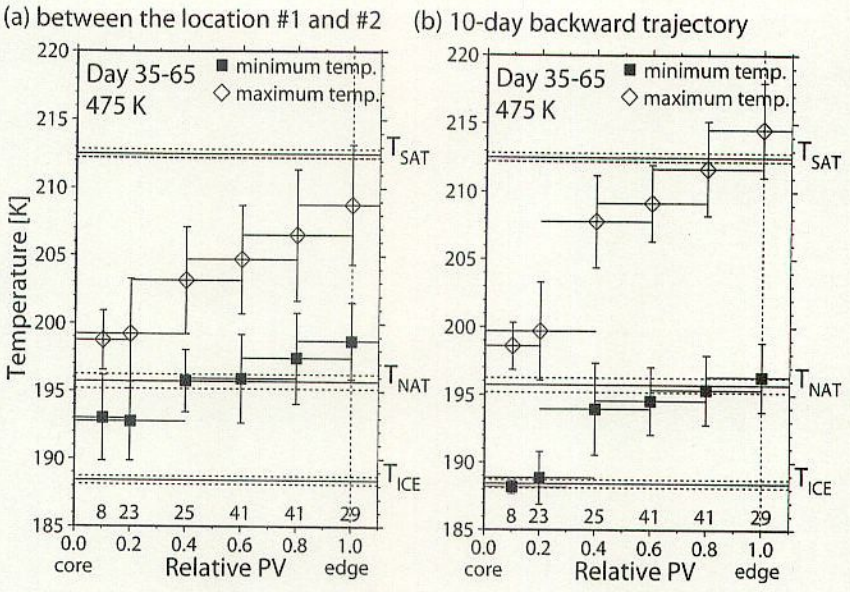

Figure 14. Minimum temperatures (solid square) and maximum temperatures (open diamond) experienced along (a) a central forward trajectory between locations 1 and 2 and (b) a 10-day central backward trajectory, which started from location 1 as a function of rPV. Horizontal lines show the SAT melting temperature and the NAT and ice PSC forming temperatures (see text). Each data point is calculated as the average for double-sounded air parcels obtained in the rPV belts of 0.0–0.2, 0.0–0.4, 0.2–0.6, 0.4–0.8, 0.6–1.0, and 0.8–1.2, respectively, from 4 February to 6 March at 475 K. Vertical error bars represent 1 sigma.

undergo a temperature below T_{NAT} between two matching soundings and experienced a temperature near T_{ice} in the past 10 days. In the middle part of the vortex (0.4 and 0.6 rPV belts), the minimum temperature on TH-B is just below T_{NAT} and never reaches T_{ice}, and that on TH-F is near T_{NAT}. On the contrary, the less ozone loss is derived near the vortex edge (0.8 and 1.0 rPV belts), in which the air parcels experience the minimum temperature near or slightly above T_{NAT} on TH-B and above T_{NAT} on TH-F. We can also see differences between the interior of the vortex and the vortex boundary region in terms of the maximum temperature: the maximum temperature is always below T_{SAT} on both TH-F and TH-B from 0.1 to 0.6 rPV belts, while near the vortex edge the maximum temperature is well below T_{SAT} on TH-F but near or above T_{SAT} on TH-B.

[38] The lower minimum temperature and the higher maximum temperature on TH-B than those on TH-F may result from the geographical differences in the route of their trajectories and the differences in the duration for their trajectories. Figures 15a and 15b show the forward trajectories between locations 1 and 2 (associated with TH-F) and the 10-day backward trajectories from location 1 (associated with TH-B), respectively, on the 475 K surface during February. The top, middle, and bottom panels show the trajectories for the double-sounded air parcels that are obtained in the vortex core region, in the middle part of the vortex, and in the vortex boundary region, respectively. For the double-sounded air parcels near the vortex core region and in the middle part of the vortex, a large number of backward trajectories pass through near the center of the vortex, the lowest temperature region, whereas the forward trajectories do not cross the vortex core region so often with some exceptions. This may be a possible reason for the lower minimum temperature on TH-B than on TH-F. One of the causes for the difference of the trajectory routes is that the backward trajectory can pass anywhere, whereas the forward trajectory must end with the location 2 which is located at almost the same latitude as the location 1. Thus, the trajectory crossing the center of the vortex between the two matching soundings may be rare because the prevailing wind is zonal.

[39] Another possible reason for the lower minimum temperatures experienced on TH-B than those on TH-F may be that the 10-day backward trajectory is always longer than the forward trajectory between the two matching observations. On the average the duration time of the trajectory between matches (TH-F) is about 3 days in this case. A possibility that the trajectory travels over either a lower temperature region or a higher temperature region increases with its duration time. The longer duration time of TH-B could also cause the higher maximum temperature on TH-B than on TH-F. In fact, the 10-day backward trajectories pass even over the lower latitude region, which is a higher temperature region, in contrast to the forward trajectories. Figure 15 also suggests that the trajectories between the matching pairs (TH-F) may not provide a reasonable "geographical" coverage of the entire vortex and hence a poor sampling of cold temperatures, although they may give a reasonable sampling of rPV values.

5. Discussions

5.1. Sensitivity of Ozone Change Rate to Analysis Parameters

[40] Errors are introduced randomly and systematically during the analysis. Random errors from any cause appear on each matching pair of observations and give the uncertainties in the ozone change rates. The statistical uncertainty

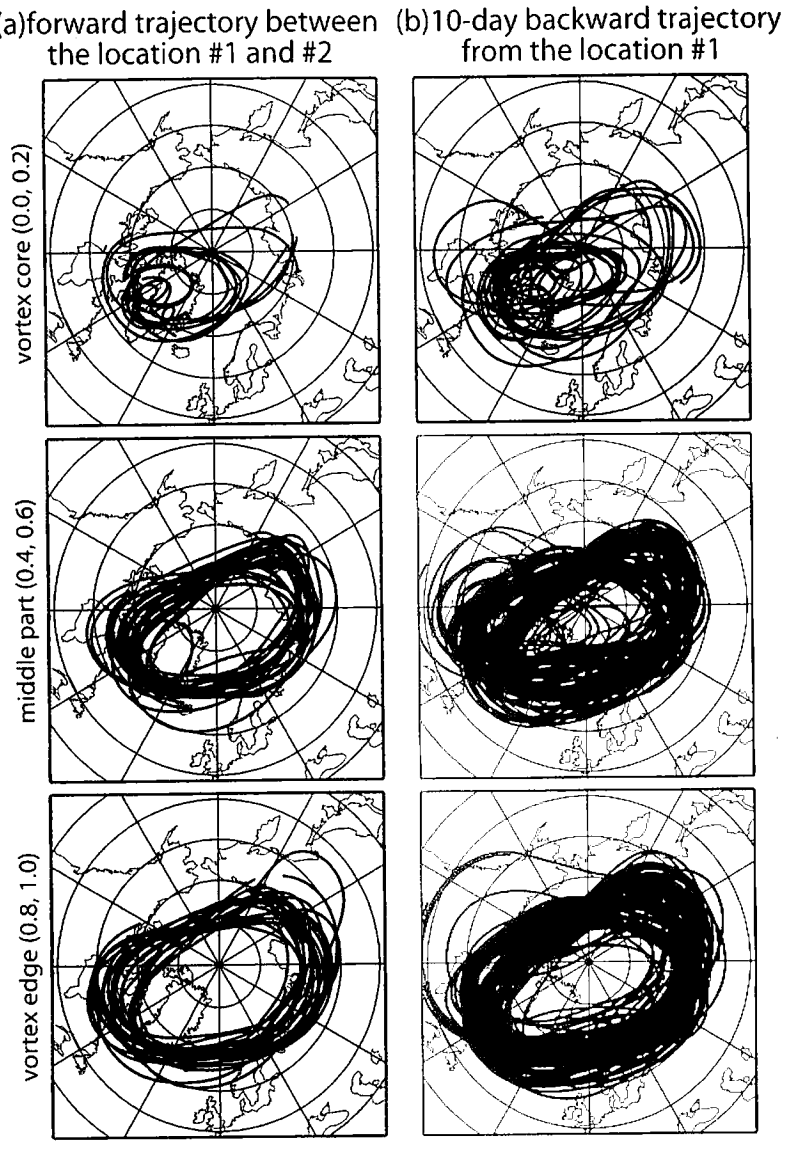

Figure 15. (a) Forward trajectories between locations 1 and 2 and (b) 10-day backward trajectories from location 1 for the double-sounded air parcels obtained around the vortex center (top panels), in the middle part of the vortex (middle panels), and in the vortex boundary region (bottom panels) during February at 475 K. Figures in the parentheses indicate the range of rPV of the double-sounded air parcels in each panel.

of ozone changes in individual double-sounded air parcels (ΔO_3^* in Figure 6) was estimated to be about 7% during February at 475 K. As main causes of systematic error, we discuss the dependence of ozone change rate on several parameters used in the analysis in this section.

[41] One of the possible sources of systematic error is the diabatic descent rate. Figure 16 shows the ozone change rates (ppbv/sunlit hour) averaged inside the inner vortex edge at the 475 K level as calculated by using 0%, 50%, and 150% cooling rates of the ones used in section 4. The magnitude of diabatic cooling rate influences the ozone change rate significantly only in early February, but much less after mid-February even though the given cooling was extreme. The lower sensitivity to the cooling rate implies that the vertical gradients of the ozone mixing ratio obtained by ILAS near the 475 K level were relatively small. Matches with a strong vertical ozone gradient would be more sensitive to diabatic descents and to small-scale vertical diffusion processes [*Rex et al.*, 1998]. Above 475 K, a significant difference in the ozone change rate was also found occasionally during late February and March (not shown here), but the magnitudes of difference were similar to those as seen in early February at 475 K. Hence, the influence on the local ozone change rate by the diabatic cooling rate is not important in this study.

[42] On the other hand, the uncertainties in the diabatic cooling rate may affect the amount of ozone loss as integrated along the descending motion of the air masses during a long period (Figure 3b). However, the effect was very small for the potential temperature surface on which the maximum ozone loss was observed. For example, even if we consider very large biases of ±50% cooling, the integrated ozone loss from 30 January to 31 March is 2.0 ± 0.1 ppmv (529–475 K, original cooling rate), 1.9 ± 0.1 ppmv (556–475 K, 150% cooling rate),and 2.1 ± 0.1 ppmv (501–475 K, 50% cooling rate).

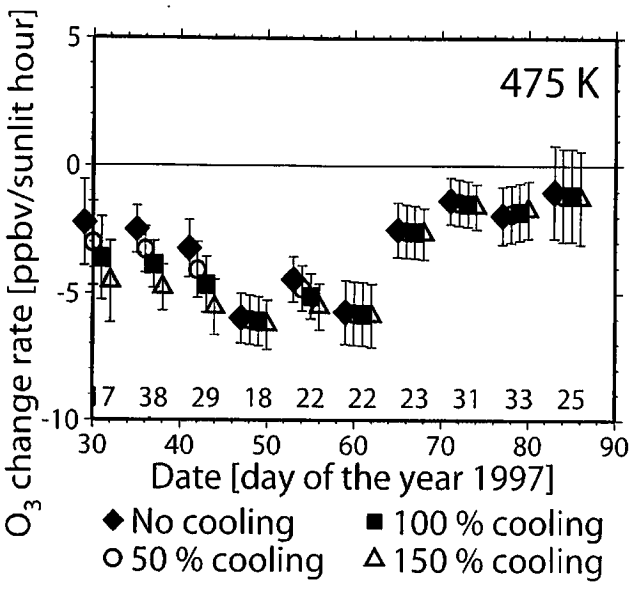

Figure 16. Time series of ozone change rates (in ppbv per sunlit hour) inside the inner edge of the vortex boundary on the 475 K potential temperature surface for different diabatic descent rates. Solid squares represent the ozone change rates as calculated with the cooling rates originally from the work of *Knudsen et al.* [1998], which are used in this paper. Open circles and open triangles depict the ozone change rates with 50% and 150% of the cooling rates, respectively. Solid diamonds show the ozone change rates without cooling. Figures at the bottom show the number of double-sounded air parcels used for the regression analysis. Results are plotted every 6 days. Diamonds, circles, and triangles are shifted horizontally for the sake of clarity. Error bars denote 1 sigma.

[43] The more essential factor that may affect the uncertainties with respect to the ozone change rates is how the double-sounded air parcels are defined. As described in section 3.1, the present study introduced ten forward and backward trajectories in total for searching a matching observation, while our preliminary study [*Sasano et al.*, 2000] and the Match 91/92 [*von der Gathen et al.*, 1995; *Rex et al.*, 1998] used only a single forward trajectory. Although six additional forward trajectories were introduced in the sonde-Match analysis from 1994/95 winter onwards [*Rex et al.*, 1999], there was little discussion on the effect of this match criteria on derived ozone change rates. We investigated sensitivity of the ozone change rate to the different criteria in defining double-sounded air parcels.

[44] Figure 17 demonstrates that the ozone loss rates as derived using the multiple forward and backward trajectories (squares) are significantly higher than those using the single forward trajectory (diamonds) by a factor of approximately 2 in some cases. It is shown that the differences in ozone change rates at the 475 K level are relatively small between using the present criteria (forward/backward match radius $\leq$500 km, forward/backward cluster radius $\leq$1600 km, and ΔPV $\leq$ 20%; squares in the figure) and using the much stricter criteria (match radius $\leq$400 km, cluster radius $\leq$1200 km, and ΔPV $\leq$ 20%; circles in the figure). On the other levels we found some cases that the ozone loss rates as calculated under the stricter distance criteria become higher than those under the present criteria (not shown). However, note that the ozone change rate as determined under the stricter distance criteria is often statistically much less significant mainly because of the smaller number of double-sounded air parcels.

[45] To investigate the reason for the higher ozone loss rate found in the multiple trajectory analysis, we focused on the differences in the scatterplots for ozone mixing ratio changes in individual double-sounded air parcels between the single trajectory and the multiple trajectory analyses. Figure 18 depicts the differences of scatterplots for ozone mixing ratio changes of double-sounded air parcels between the two different criteria for defining the air parcels. The closed circles represent the data as selected by the criteria in this study, and the open circles the data selected by the single forward trajectory without the multiple trajectory analysis. By adding the criteria associated with the multiple trajectories, the data points which give a small change in ozone mixing ratio in spite of a long sunlit time (open circles after 30 sunlit hours in the figure) are filtered out, and a higher ozone loss rate is derived. Most of the filtered-out data are located in the region from 70°N to 75°N in equivalent latitude, near the vortex boundary region. Thus, the multiple trajectory analysis serves to screen out the data

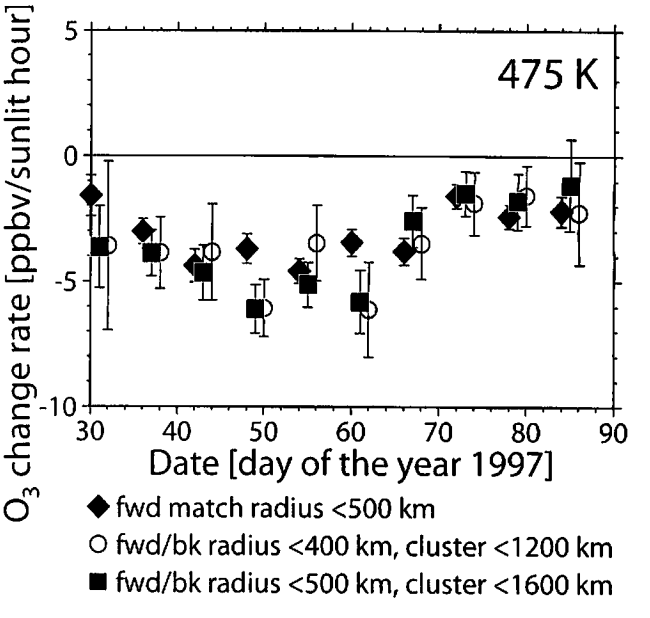

Figure 17. Time series of ozone change rates for different criteria associated with double-sounded air parcel selection. Solid squares show the ozone change rates as determined by the five criteria, i.e., both forward and backward match radius $\leq$ 500 km, both forward and backward cluster radius $\leq$ 1600 km, and ΔPV $\leq$ 20% (the same as the squares in Figure 16). Open circles depict ozone change rates as calculated with stricter distance criteria than above: both forward and backward match radius $\leq$ 400 km, both forward and backward cluster radius $\leq$ 1200 km, and ΔPV $\leq$ 20%. Solid diamonds give the ozone change rates as calculated with only two criteria: the forward match radius $\leq$ 500 km and ΔPV $\leq$ 20%.

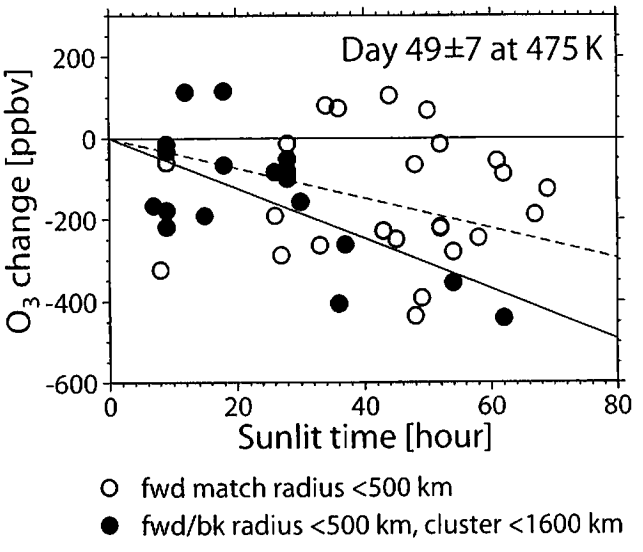

Figure 18. Differences of scatterplots for ozone mixing ratio change between two different criteria for selecting double-sounded air parcels. Closed circles depict the ozone mixing ratio change as selected by the criteria of the forward/backward match radius $\leq$ 500 km, the forward/backward cluster radius $\leq$ 1600 km, and ΔPV $\leq$ 20%, and the solid line indicates the ozone change rate derived from the subset of closed crosses (the same as Figure 7). Open circles depict the additional data, which satisfy only the criteria of the forward match radius and ΔPV, and the dashed line indicates the ozone change rate derived from all data points (-3.9 ± 0.6 ppbv/sunlit hour). Conditions are the same as in Figure 7 in every other respect.

near the vortex edge selectively, possibly because the cluster of trajectories tends to diverge near the vortex edge where the horizontal and vertical wind shear are larger than in the interior of the vortex. In this situation, the backward trajectories were also hardly able to return to near the first soundings. The multiple trajectories thus help to identify accurately the double-sounded air masses.

[46] As described in section 2, we eliminated the ozone data that may have been affected by PSCs occurrence because the ILAS gas values could have been biased even after applying the nongaseous correction when PSCs existed at the same time. A total of 30 (17) double-sounded air parcels was discarded in February (March), which are 3–5% of the total number of the air parcels (see Table 2). If the double-sounded air parcels that included PSCs were added to the analysis, the ozone change rates averaged inside the inner vortex edge became 50–70 ppbv/day at the maximum during late February at 450–500 K levels, which were slightly smaller than the present study (50–80 ppbv/day). The same analysis shows that the integrated ozone loss at 475 K during 2 months was 1.9 ± 0.1 ppmv and the column ozone loss was 94 ± 0.3 DU. These are very slightly smaller compared to the analysis in section 4.1 (2.0 ± 0.1 ppmv and 96 ± 0.3 DU, respectively).

5.2. Relationship Between Ozone Loss and Low Temperature

[47] The 1996/1997 Arctic winter to spring polar vortex was very strong and symmetric about the North Pole, and the stratospheric temperature was low enough for PSCs to exist [e.g., *Coy et al.*, 1997; *Pawson and Naujokat*, 1999]. Such low temperature likely forms PSCs, and then rapidly produces reactive chlorine through heterogeneous reactions on the surface of PSCs. The reactive chlorine destroys catalytically ozone under sunlit conditions [*Solomon et al.*, 1986]. The identification of PSCs from aerosol extinction coefficient profiles at 780 nm of the ILAS observations confirmed that PSCs existed in the Arctic stratosphere during January, February, and early March [*Hayashida et al.*, 2000; *Saitoh et al.*, 2002]. The large ozone loss happened to coincide with the occurrence of PSCs [*Sasano et al.*, 2000] and the very low temperature that appeared on the temperature histories (Figure 13), which supports the general idea that the very low temperature and consequently the PSCs caused the large ozone losses during early spring.

[48] The temperature history can be regarded as an indicator of PSCs formation and phase transition. PSC types are critical to ozone losses because only solid particles can cause denitrification which prolongs the chemical ozone destruction [e.g., *Salawitch et al.*, 1993; *Rex et al.*, 1997] and because the heterogeneous reaction rates vary depending on the chemical composition of the particles [e.g., *Peter*, 1997]. One view of temperature history in the PSC particles cycle is briefly as follows [*Koop et al.*, 1997; *Peter*, 1997; *Larsen*, 2000]: Liquid sulfate aerosol stake up nitric acid and water vapor with decreasing temperature and turn into supercooled ternary solutions (STS) as type Ib PSCs below T_{NAT}. Then, water freezes below T_{ice}, hence type II PSCs are formed, and the nucleation of NAT takes place on the ice by deposition. As the temperature rises above T_{ice}, ice will evaporate and only NAT will remain (type Ia PSC), which will evaporate above T_{NAT} and turn into SAT. Once SAT particles are produced, they exist until the temperature rises above about T_{SAT}, or they turn into NAT and type II PSCs if the temperature decrease again.

[49] According to this scenario, Figure 14 suggests two points. The first point is that type Ia PSCs could exist between some of the two matching observations in the deep part of the vortex (0.1 and 0.2 rPV belts), because the temperature within 10 days prior to the matches drops near T_{ice} and the temperature between the matches is almost below T_{NAT}. Although the above mechanisms require the temperature to be 2–3 K below T_{ice}, the statistical analysis of synoptic temperature histories of PSCs indicated that synoptic temperatures below T_{ice} are not necessary for type Ia PSCs formation [*Larsen et al.*, 1997]. Recent studies present other NAT formation scenarios including homogeneous nucleation of NAT near 190 K [*Tolbert and Toon*, 2001]. *Fahey et al.* [2001] observed very large NAT particles ("NAT rocks") where no ice clouds were observed or predicted. The trajectories of NAT rocks shows that these particles grow above T_{ice} by a few degrees. These studies support that the minimum temperature near T_{ice} within 10 days prior to the matches might be low enough for solid PSCs to form. Actually, the ILAS nitric acid data demonstrated denitrification during mid-February to early March at this altitude [*Kondo et al.*, 2000], and the magnitude of denitrification was larger at a higher equivalent latitude with the maximum at 80° equivalent latitude [*Irie et al.*, 2001]. The microwave Limb Sounder (MLS) instrument on board the UARS illustrated that enhanced ClO filled a smaller

portion inside the vortex and the largest ClO values appeared near the vortex core region around the 475 K level [*Santee et al.*, 1997]. These evidences strongly suggest that the double-sounded air parcels obtained in the innermost part of the vortex were exposed to type Ia PSCs, and experienced denitrification and extreme ozone losses.

[50] The second point is that type Ib PSCs could exist between the two matching observations near the vortex boundary region (0.8 and 1.0 rPV belts), because the temperature within 10 days prior to the matches experiences below or near T_{NAT} but never falls below T_{ice}, and the temperature between the matches is almost above T_{NAT} by a few degrees. Type Ib PSCs may cause smaller ozone loss without denitrification, compared to near the vortex core region. In the middle part of the vortex (0.4 and 0.6 rPVs), the formation of NAT particles between the two matching observations may have been difficult because the minimum temperatures on trajectories seem too high, even if homogeneous nucleation or NAT rocks scenario is taken into consideration. The formation of type Ib PSCs between matches may be possible also in the middle part of the vortex.

5.3. Comparison With Other Studies

[51] Several other studies investigated the stratospheric ozone loss during the 1996/1997 Arctic winter, though here we discuss mainly the results which give purely chemical ozone loss rates and amounts in 1996/1997 winter–spring. In this study we presented two kinds of estimation for vortex-averaged ozone change rates, i.e., the average inside the inner edge of the vortex boundary region (section 4.1) and the average inside the vortex edge (section 4.3). Most of other studies used the data inside the vortex edge, rather than the inner vortex edge, for calculating vortex-averaged ozone change rates. Therefore, the ozone change rates as averaged inside the vortex edge are employed here for comparison with other studies.

[52] *Schulz et al.* [2000] presented the chemical ozone loss rates as determined by the 1996/1997 Match experiment. The pattern of ozone changes by them is similar to the one from the present study. They showed that the vortex-averaged ozone loss rates were from 25 to 45 ppbv/day at the maximum, the column ozone loss (mainly from 400 to 520 K between 1 February and 26 March) was 43 ± 9 DU, and the integrated ozone loss was 0.9 ± 0.2 ppmv on the 450 K surface. The ozone change rates inside the vortex edge in this study are 20–50 ppbv/day at 475 K (diamonds in Figure 12). As for the column ozone loss, the time and range of the column for integration were adjusted to those of Schulz et al. and the column ozone loss was reevaluated from this study, resulting in 56 ± 0.3 DU. The integrated ozone loss between 1 February and 26 March was 1.3 ± 0.1 ppmv on the 450 K surface. These results shows that the vortex-averaged ozone losses derived from the present study are a little larger than those from the sonde-Match analysis. The definition of the vortex edge (about 37 PVU at 475 K) is similar to that used in the sonde-Match analysis (36 PVU at 475 K). The change of ozone loss rate with the relative location to the vortex were qualitatively consistent with each other. Their ozone loss rate of about 6 ppbv/sunlit hour at the vortex core region (from 10 February to 10 March at 450–500 K) quantitatively agrees with our result in Figure 11 (from 4 February to 6 March at 475 K). On the other hand, for the other part of the vortex, the ozone loss rates in our study are higher than that of Schulz et al.

[53] There are some differences between the ILAS-Match and the sonde-Match not only in the data source (ozonesonde or satellite measurement) but also in the details of the analysis method (e.g., trajectory calculation tool, match criteria, definition of the vortex boundary, and diabatic cooling rate). One of the reasons for the differences in the vortex-averaged ozone loss may have arisen from the relative position of the matches to the vortex. As discussed previously, the multiple trajectory analysis in this study selectively eliminated the unreliable matches near the vortex edge, thus making the vortex-averaged ozone loss rate higher. In addition, we used more matching observations in the deep part of the vortex than the sonde-Match analysis (compare Figure 8 and Figure 10 in this paper with Figure 3 in the work of *Schulz et al.* [2000]) to calculate the vortex-averaged ozone loss rate. In this study a lot of sampling existed near the vortex core region during February and March, while for the sonde-Match analysis only few matches were obtained in the vortex core region during March. In fact, the ozone loss rates, as calculated inside the vortex edge but without near the vortex core region (i.e., from 1.0 to 0.4 rPVs, which is a similar range used in the sonde-Match), are 15–20 ppbv/day in March, which is comparable to the sonde-Match results. Another possible factor for the differences between the ILAS-Match and the sonde-Match approach is solar zenith angles (SZAs) on trajectories. The differences in the geographical location of the trajectories may produce differences in the SZAs and also in the photolysis rates.

[54] *Müller et al.* [1997] identified chemical ozone depletion using the correlation between ozone and long-lived tracer gases observed by HALOE on UARS, and estimated the column ozone loss as 50–80 DU between 350 and 550 K, varying with the location inside the vortex. When we put an upper limit of the vertical integration to 550 K and a lower limit to 375 K in our analysis, the column ozone loss becomes 81 ± 0.4 DU, which is close to the result by Müller et al. They also suggested that the larger ozone losses tended to occur toward the vortex interior. This in homogeneity is qualitatively consistent with our results.

[55] *Manney et al.* [1997] used MLS observations and transport estimations to deduce the degree of chemical ozone depletion. The ozone losses between 20 and 26 February were 1.3%/day (34 ppbv/day) at 465 K. Their result is in good agreement with the vortex-averaged ozone loss rates of 32 ppbv/day at 465 K from our analysis, as averaged over the same period.

[56] *Knudsen et al.* [1998] calculated vortex-averaged ozone depletions on several potential temperature surfaces using ozonesonde data and reverse domain-filling trajectory calculations, taking the effect of transport into account. The integrated chemical ozone loss from 30 January to 31 March was 1.0 ppmv at 400 K and 1.3 ppmv at 450 K. The integrated ozone loss in the present study, 1.1 ppmv at 400 K and 1.6 ppmv at 450K, is slightly higher than the results of Knudsen et al., possibly because of the difference in the distribution of the sounding location between the ozonesonde and the ILAS. Their average column ozone loss of 79 DU (from 375 to 550 K) were comparable to our results, 81 ± 0.4 DU (the same vertical region).

[57] *Braathen et al.* [2000] also calculated ozone depletion from the time series of the ozone mixing ratio observed by the ozonesonde, which was corrected by diabatic cooling rate but ignoring the transport effects. The local ozone change rates were 15–30 ppbv/day during late February and early March at 475 K, and the integrated ozone depletion was about 1.6 ppmv during 2 months. Using the same method as *Braathen et al.* [2000], the Global Ozone Monitoring Experiment (GOME) ozone profiles indicated ozone depletion of about 1.5 ppmv during the same period and at the isentropic surface [*Bramstedt et al.*, 2000]. Although the technique used in these studies could not derive purely chemically induced ozone loss because dynamical ozone changes caused by the horizontal advection of air masses were ignored, these estimations give relatively similar ozone losses to the present study.

[58] Three-dimensional Chemistry Transport Models (CTM) also provided estimates of the Arctic ozone loss. The integrated ozone loss as simulated by SLIMCAT [*Guirlet et al.*, 2000] is 36% at 480 K on 31 March over north of 75°N equivalent latitude, which underestimates the integrated ozone loss averaged inside the inner vortex edge (north of 70°N equivalent latitude), 55% at 475 K in the present study. As for the column ozone loss, our result is within the estimations by the Reprobus CTM, which vary from 60 to 120 DU loss with the location inside the vortex [*Lefèvre et al.*, 1998].

6. Summary

[59] In this paper we evaluated quantitative chemical ozone loss rates and amounts in the Arctic stratospheric vortex for the spring of 1997 using the ILAS newest ozone profile data (Version 5.20) and the Satellite-Match analysis.

[60] The analysis method is an extension of the Match technique. The advantages of using the ILAS data are that the ILAS measurements intensively cover all longitudinal regions in the high latitude zone, ILAS is performed daily all with the same quality, and ILAS provides not only ozone data but also data on nitric acid and passive tracers so that further comprehensive analysis [*Terao et al.*, 2000] is possible. In order to overcome the disadvantages of satellite sensor data, low vertical resolution and larger sampling air mass volume, the analysis method was improved and very strict criteria assuring conservation of air masses were introduced to identify a double-sounded air mass more reliably. For this purpose, we calculated multiple trajectories for each ILAS observation, including central forward/backward trajectories and a cluster of four forward/backward trajectories (Figures 2, 4 and 5). Based on the multiple trajectory analysis, several hundred double-sounded air parcels were identified between 375 and 600 K potential temperature surfaces during February and March (Table 2). We statistically calculated chemical ozone change rates by regression analysis on the subset of double-sounded air parcels taking into account the diabatic descent. The statistical uncertainty of ozone changes was estimated to be about 7% in this analysis. In the analysis the derived ozone change rates were less sensitive to uncertainties in diabatic descent rate.

[61] Using the double-sounded air parcels obtained inside the inner edge of the vortex boundary (corresponding to north of about 70°N equivalent latitude), vortex-averaged ozone loss rates were evaluated (Figure 9). The result shows that the local maximum ozone loss rate was 50–80 ppbv/day during late February at 450–500 K levels. The integrated ozone loss during February and March was 2.0 ± 0.1 ppmv at 475–529 K levels, and the column ozone loss between 400 and 600 K during the 2 months was 96 ± 0.3 DU. We also studied the relationship between the ozone loss rate and the location relative to the vortex (Figure 11). The ozone change rates as a function of rPV demonstrated that the ozone loss increased toward the vortex center with a step-like increase at 0.2 rPV (about 80°N equivalent latitude). The magnitude of ozone loss is strongly dependent on relative location to the vortex in this winter. The higher ozone loss in the deeper part of the vortex is consistent with other studies [*Müller et al.*, 1997; *Manney et al.*, 1997; *Lefèvre et al.*, 1998; *Guirlet et al.*, 2000; *Schulz et al.*, 2000]. The maximum ozone loss rate of 6.0 ± 0.6 ppbv/sunlit hour near the vortex core region was also quantitatively in agreement with the sonde-Match analysis.

[62] When we expanded the area of interest to include all the data obtained inside the vortex edge (north of about 65 °N equivalent latitude), the local ozone loss rate was about 50 ppbv/day at the maximum. The integrated ozone change during 2 months is 1.6 ± 0.1 ppmv on the 475–529 K surfaces and the column ozone loss between 400 and 600 K during the 2 months is 72 ± 0.4 DU. The vortex-averaged ozone loss inside the vortex edge is in agreement with those of several other studies [*Manney et al.*, 1997; *Müller et al.*, 1997; *Knudsen et al.*, 1998; *Lefèvre et al.*, 1998], but is slightly larger than the 96/97 Match results [*Schulz et al.*, 2000] and our previous analysis [*Sasano et al.*, 2000] by about 10 ppbv/day. One of the reasons for the differences in the vortex-averaged ozone loss may have arisen from the relative position of the matches to the vortex. The multiple trajectory analysis selectively eliminated the case of matching observations near the vortex edge. Thus the vortex-averaged ozone loss rate as determined in this study likely reflects the higher local ozone loss deep inside the vortex. In addition, we obtained more matching observations in the deep part of the vortex in March than the sonde-Match analysis. In fact, the ozone loss rates, as calculated in a similar vortex range used in the sonde-Match, are comparable to the sonde-Match results.

[63] Temperature histories of a corresponding double-sounded air parcel indicated that large ozone losses in the innermost part of the vortex were observed when the air parcels reached a temperature below T_{NAT} between the two matching soundings and had experienced a temperature near T_{ice} within the 10 days prior to the soundings. Considering the phase transition cycle of PSCs [*Koop et al.*, 1997; *Peter*, 1997; *Larsen*, 2000; *Fahey et al.*, 2001; *Tolbert and Toon*, 2001], this temperature history suggests that type Ia PSCs could have existed deep inside the vortex during the period when the extremely large ozone loss occurred.

[64] **Acknowledgments.** The authors express their sincere thanks to Richard Swinbank for supplying the UKMO assimilation data and trajectory programs, Bjørn M. Knudsen for providing his diabatic cooling rate data, and Naoko Saitoh and Sachiko Hayashida for providing their PSCs analysis data. We are also grateful to Peter von der Gathen, Takafumi Sugita, and the anonymous referees for their helpful comments and discussions. The ILAS data were processed at the ILAS/ILAS-II Data Handling Facility (DHF), National Institute for Environmental Studies

(NIES). The ILAS data were made available by the tremendous efforts of the ILAS project staff, to whom the authors are greatly obliged.

References

Braathen, G., I. Kilbane-Dawe, E. Kyrö, P. von der Gathen, I. S. Mikkelsen, V. Dorokhov, H. Fast, and M. Gil, Temporal evolution of ozone in the Arctic vortex during the winters from 1988–89 to 1998–99, *Proceedings of the 5th European Symposium on Stratospheric Ozone, Saint Jean de Luz*, pp. 411–416, 2000.

Bramstedt, K., K.-U. Eichmann, M. Weber, R. Hoogen, V. Rozanov, and J. P. Burrows, Chemical ozone depletion during Arctic spring seasons 1996/97–1998/99 derived from Northern Hemispheric GOME ozone profile distribution, *Proceedings of the 5th European Symposium on Stratospheric Ozone, Saint Jean de Luz*, pp. 417–420, 2000.

Coy, L., E. R. Nash, and P. A. Newman, Meteorology of the polar vortex: Spring 1997, *Geophys. Res. Lett.*, *24*, 2693–2696, 1997.

Chubachi, S., Preliminary result of ozone observations at Syowa station from February 1982 to January 1983, *Mem. Natl. Inst. Polar Res., Spec. Issue Jpn.*, *34*, 13–19, 1984.

Denis, L., J.-P. Pommereau, F. Lefèvre, F. Goutail, B. Knudsen, and G. Letrenne, Ozone loss and NO_2 recovery in the Arctic winter and spring of 1997 as observed from long duration balloon flights in the vortex, *Proceedings of the 5th European Symposium on Stratospheric Ozone, Saint Jean de Luz*, pp. 425–428, 2000.

Farman, J. C., B. G. Gardiner, and J. D. Shanklin, Large losses of total ozone in Antarctica reveal seasonal ClO_x/NO_x interaction, *Nature*, *315*, 207–210, 1985.

Fahey, D. W., et al., The detection of large HNO_3-containing particles in the winter arctic stratosphere, *Science*, *291*, 1026–1031, 2001.

Guirlet, M., M. P. Chipperfield, J. Pyle, F. Goutail, J.-P. Pommereau, and E. Kyrö, Modeled Arctic ozone depletion in winter 1997/1998 and comparison with previous winters, *J. Geophys. Res.*, *105*, 22,185–22,200, 2000.

Hansen, G., and M. P. Chipperfield, Ozone depletion at the edge of the Arctic polar vortex 1996/1997, *J. Geophys. Res.*, *104*, 1837–1845, 2000.

Hanson, D., and K. Mauersberger, Laboratory studies of the nitric acid trihydrate: Implications for the south polar stratosphere, *Geophys. Res. Lett.*, *15*, 855–858, 1988.

Hayashida, S., N. Saitoh, A. Kagawa, T. Yokota, M. Suzuki, H. Nakajima, and Y. Sasano, Arctic polar stratospheric clouds observed with the Improved Limb Atmospheric Spectrometer during winter 1996/1997, *J. Geophys. Res.*, *105*, 24,715–24,730, 2000.

Irie, H., M. Koike, Y. Kondo, G. E. Bodeker, M. Y. Danilin, and Y. Sasano, Redistribution of nitric acid in the Arctic lower stratosphere during the winter of 1996–1997, *J. Geophys. Res.*, *106*, 23,139–23,150, 2001.

Knudsen, B. M., et al., Ozone depletion in and below the Arctic vortex for 1997, *Geophys. Res. Lett.*, *25*, 627–630, 1998.

Koop, T., K. S. Carslaw, and T. Peter, Thermodynamic stability and phase transitions of PSC particles, *Geophys. Res. Lett.*, *24*, 2199–2202, 1997.

Kondo, Y., H. Irie, M. Koike, and G. E. Bodeker, Denitrification and nitrification in the Arctic stratosphere during the winter of 1996–1997, *Geophys. Res. Lett.*, *27*, 337–340, 2000.

Larsen, N., B. M. Knudsen, J. M. Rosen, N. T. Kjome, R. Neuber, and E. Kyrö, Temperature histories in liquid and solid polar stratospheric cloud formation, *J. Geophys. Res.*, *102*, 23,505–23,517, 1997.

Larsen, N., Chemical understanding of ozone loss-heterogeneous processes: Microphysical understanding and outstanding issues, *Proceedings of the 5th European Symposium on Stratospheric Ozone, Saint Jean de Luz*, pp. 173–178, 2000.

Lefèvre, F., F. Figarol, K. S. Carslaw, and T. Peter, The 1997 Arctic ozone depletion quantified from three-dimensional model simulations, *Geophys. Res. Lett.*, *25*, 2425–2428, 1998.

Manney, G. L., L. Froidevaux, M. L. Santee, R. W. Zurek, and J. W. Eaters, MLS observations of Arctic ozone loss in 1996–97, *Geophys. Res. Lett.*, *24*, 2697–2700, 1997.

Marti, J., and K. Mauersberger, A survey and new measurements of ice vapor pressure at temperatures between 170 and 250 K, *Geophys. Res. Lett.*, *20*, 363–366, 1993.

Middlebrook, A. M., L. T. Iraci, L. S. McNeill, B. G. Koehler, M. A. Wilson, O. W. Saastad, M. A. Tolbert, and D. R. Hanson, Fourier transform-infrared studies of thin H_2SO_4/H_2O films: Formation, water uptake, and solid–liquid phase changes, *J. Geophys. Res.*, *98*, 20,473–20,481, 1993.

Müller, R., J.-U. Grooß, D. S. McKenna, P. J. Crutzen, C. Brühl, J. M. Russell III, and A. F. Tuck, HALOE observations of the vertical structure of chemical ozone depletion in the Arctic vortex during winter and early spring, *Geophys. Res. Lett.*, *24*, 2717–2720, 1997.

Nakajima, H., et al., Characteristics and performance of the Improved Limb Atmospheric Spectrometer (ILAS) in orbit, *J. Geophys. Res.*, *107*, doi:10.1029/2001JD001439, in press, 2002.

Nash, E. R., P. A. Newman, J. E. Rosenfield, and M. R. Schoeberl, An objective determination of the polar vortex using Ertel's potential vorticity, *J. Geophys. Res.*, *101*, 9471–9478, 1996.

Newman, P. A., J. F. Gleason, R. D. McPeters, and R. S. Stolarski, Anomalously low ozone over the Arctic, *Geophys. Res. Lett.*, *24*, 2689–2692, 1997.

Pawson, S., and B. Naujokat, The cold winters of the middle 1990s in the northern lower stratosphere, *J. Geophys. Res.*, *104*, 14,209–14,222, 1999.

Peter, T., Microphysics and heterogeneous chemistry of polar stratospheric clouds, *Annu. Rev. Phys. Chem.*, *48*, 785–822, 1997.

Pullen, S., and R. L. Jones, Accuracy of temperatures from UKMO analyses of 1994/95 in the arctic winter stratosphere, *Geophys. Res. Lett.*, *24*, 845–848, 1997.

Rex, M., et al., Prolonged stratospheric ozone loss in the 1995–96 Arctic winter, *Nature*, *389*, 835–838, 1997.

Rex, M., et al., In-situ measurements of stratospheric ozone depletion rates in the Arctic winter 1991/92: A Lagrangian approach, *J. Geophys. Res.*, *103*, 5843–5853, 1998.

Rex, M., et al., Chemical ozone loss in the arctic winter 1994/95 as determined by the Match technique, *J. Atmos. Chem.*, *32*, 35–59, 1999.

Rowland, F. S., and M. J. Molina, Chlorofluoromethanes in the environment, *Rev. Geophys. Space Phys.*, *13*, 1–35, 1975.

Saitoh, N., S. Hayashida, Y. Sasano, and L. L. Pan, Characteristics of Arctic Polar Stratospheric Clouds in the winter of 1996/1997 inferred from ILAS measurements, *J. Geophys. Res.*, *107*, doi:10.1029/2001JD000595, in press, 2002.

Salawitch, R. J., et al., Chemical loss of ozone in the Arctic polar vortex in the winter of 1991–1992, *Science*, *261*, 1146–1149, 1993.

Santee, M. L., G. L. Manney, L. Froidevaux, R. W. Zurek, and J. W. Waters, MLS observations of ClO and HNO_3 in the 1996–97 Arctic polar vortex, *Geophys. Res. Lett.*, *24*, 2713–2716, 1997.

Sasano, Y., M. Suzuki, T. Yokota, and H. Kanzawa, Improved Limb Atmospheric Spectrometer (ILAS) for stratospheric ozone layer measurements by solar occultation technique, *Geophys. Res. Lett.*, *26*, 197–200, 1999.

Sasano, Y., Y. Terao, H. L. Tanaka, T. Yasunari, H. Kanzawa, H. Nakajima, T. Yokota, H. Nakane, S. Hayashida, and N. Saitoh, ILAS observations of chemical zone loss in the Arctic vortex during early spring 1997, *Geophys. Res. Lett.*, *27*, 213–216, 2000.

Schulz, A., et al., Match observations in the Arctic winter 1996/97: High stratospheric ozone loss rates correlate with low temperatures deep inside the polar vortex, *Geophys. Res. Lett.*, *27*, 205–208, 2000.

Sinnhuber, B.-M., J. Langer, U. Klein, U. Raffalski, K. Künzi, and O. Schrems, Ground based millimeter-wave observations of Arctic ozone depletion during winter and spring of 1996/97, *Geophys. Res. Lett.*, *25*, 3327–3330, 1998.

Solomon, S., R. R. Garcia, F. S. Rowland, and D. J. Wuebbles, On the depletion of Antarctic ozone, *Nature*, *321*, 755–758, 1986.

Sugita, T., et al., Validation of ozone measurements from the Improved Limb Atmospheric Spectrometer (ILAS), *J. Geophys. Res.*, *107*, doi:10.1029/2001JD000602, in press, 2002.

Swinbank, R., and A. O'Neill, A stratosphere–troposphere data assimilation system, *Mon. Weather Rev.*, *122*, 1560–1570, 1994.

Terao, Y., H. L. Tanaka, T. Yasunari, and Y. Sasano, ILAS observations of chemical ozone loss and changes in nitric acid and nitrous oxide concentrations in the Arctic vortex during early spring 1997, *Proceedings of the Quadrennial Ozone Symposium, Sapporo*, pp. 111–112, 2000.

Tolbert, M. A., and O. B. Toon, Solving the PSC mystery, *Science*, *292*, 61–63, 2001.

von der Gathen, P., et al., Observational evidence for chemical ozone depletion over the Arctic in the winter 1991–92, *Nature*, *375*, 131–134, 1995.

World Meteorological Organization (WMO), *Scientific Assessment of Ozone Depletion: 1998*, Global Ozone Research and Monitoring Project, Report No. 44, Geneva, 1999.

Yokota, T., H. Nakajima, T. Sugita, H. Tsubaki, Y. Itou, M. Kaji, M. Suzuki, H. Kanzawa, J. H. Park, and Y. Sasano, Improved Limb Atmospheric Spectrometer (ILAS) data retrieval algorithm for Version 5.20 gas profile products, *J. Geophys. Res.*, *107*, doi:10.1029/2001JD000628, in press, 2002.

H. L. Tanaka, Y. Terao, and T. Yasunari, Institute of Geoscience, University of Tsukuba, Tsukuba, Ibaraki 305-8571, Japan. (terao@luft.geo.tsukuba.ac.jp)

H. Nakajima and Y. Sasano, National Institute for Environmental Studies, Tsukuba, Ibaraki 305-0053, Japan.

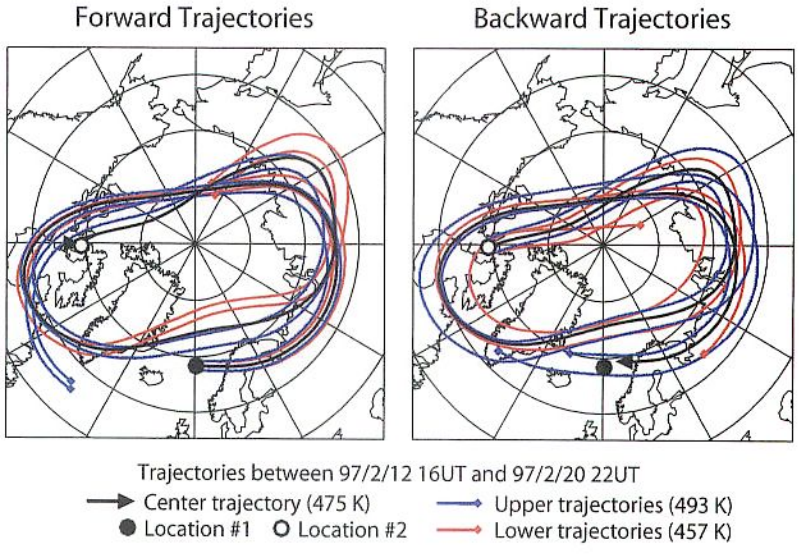

Figure 4. Example of a cluster of forward (left) and backward (right) trajectories between 12 and 20 February 1997. A thick black curve with an arrow shows a center trajectory on the 475 K potential temperature surface. Blue and red trajectories are at the upper level (493 K) and the lower level (457 K), respectively, and small solid circles show the end of each trajectory.

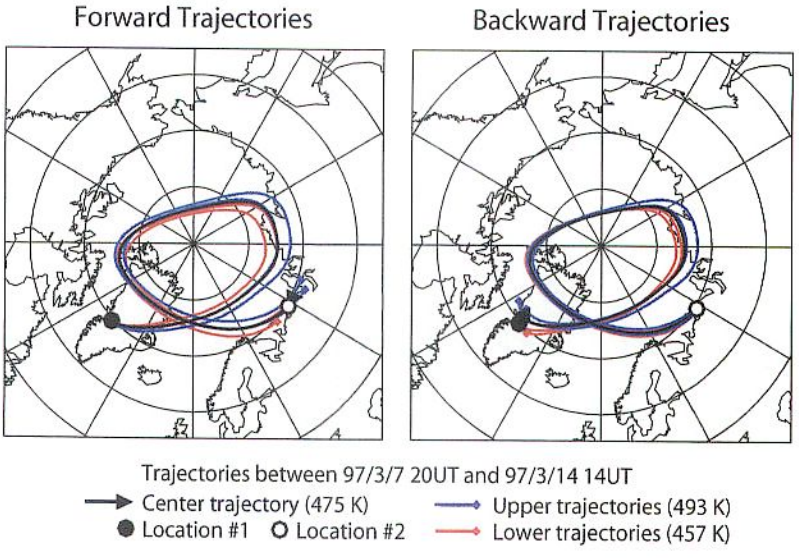

Figure 5. Same as in Figure 4, but between 7 and 14 March 1997.

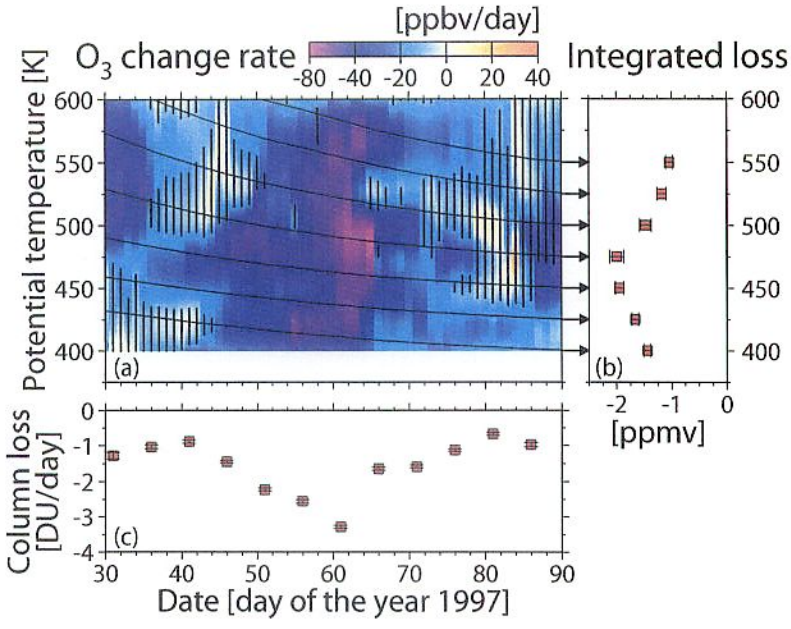

Figure 9. (a) Color-coded ozone change rates (in ppbv per day) inside the inner edge of the vortex boundary (north of about 70 °N equivalent latitude) as a function of potential temperature and date. Vertical bars indicate the region with statistical significance less than 99%. Smooth thin curves show potential temperature changes of air parcels (diabatic descent of air masses) (adopted from the work of *Knudsen et al.* [1998]). (b) Integrated ozone changes from 30 January (day 30) to 31 March (day 90) along the descending motion due to diabatic cooling. For the integration, ozone change rates are vertically interpolated by a cubic spline. For the uppermost two levels, days 51–90 and days 37–90 are used for the integration, respectively. Error bars represent 1 sigma. (c) Ozone column change rates (in DU per day), which are obtained by integrating local ozone change rates (in number density per day) from 400 to 600 K. Results are plotted every 5 days.

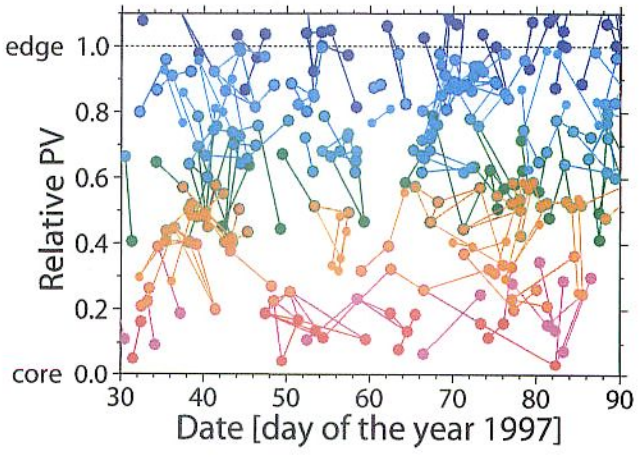

Figure 10. Location of double-sounded air parcels obtained in each rPV belt. In the rPV scale, 0 refers to the center of the vortex where the PV value takes the maximum and 1 refers to the vortex edge (see text). Red, magenta, orange, green, cyan, and blue indicate the double-sounded air parcels in the rPV belts of 0.0–0.2, 0.0–0.4, 0.2–0.6, 0.4–0.8, 0.6–1.0, and 0.8–1.2, respectively.